

53  
12/7/94 YS(2)

PREPARED FOR THE U.S. DEPARTMENT OF ENERGY,  
UNDER CONTRACT DE-AC02-76-CHO-3073

PPPL-3023  
UC-420,426

PPPL-3023

$\beta$  LIMIT DISRUPTIONS IN THE TFTR TOKAMAK

BY

E.D. FREDRICKSON, K. MCGUIRE, A. JANOS, ET AL.

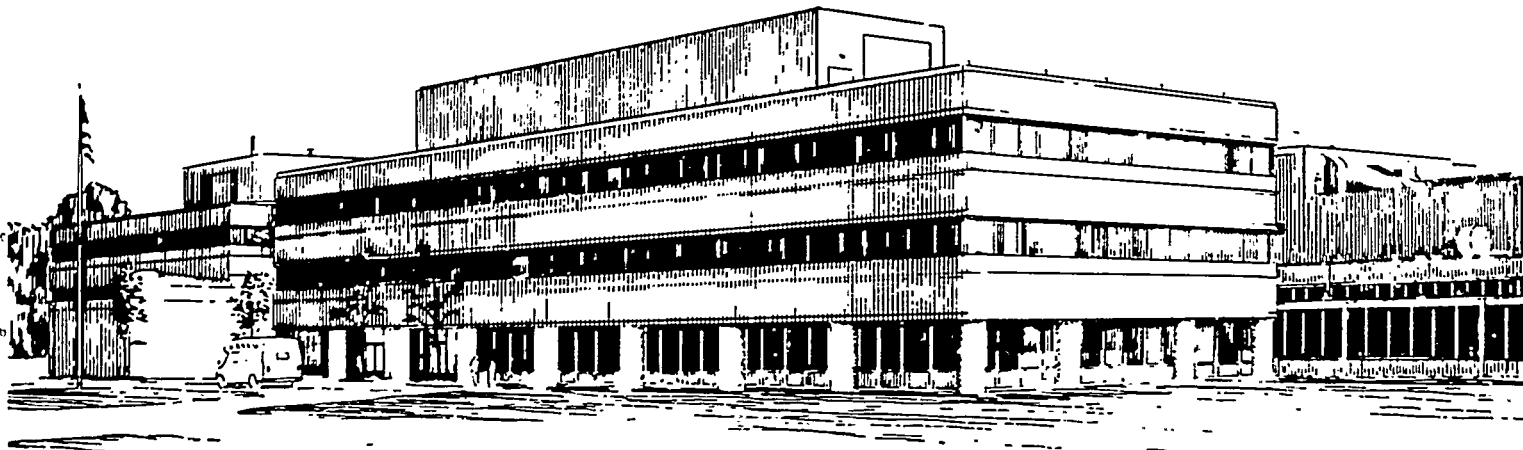
NOVEMBER 1994

MASTER

DISTRIBUTION OF THIS DOCUMENT IS UNLIMITED

YF

**PPPL** PRINCETON  
PLASMA PHYSICS  
LABORATORY



PRINCETON UNIVERSITY, PRINCETON, NEW JERSEY

## NOTICE

This report was prepared as an account of work sponsored by an agency of the United States Government. Neither the United States Government nor any agency thereof, nor any of their employees, makes any warranty, express or implied, or assumes any legal liability or responsibility for the accuracy, completeness, or usefulness of any information, apparatus, product, or process disclosed, or represents that its use would not infringe privately owned rights. Reference herein to any specific commercial produce, process, or service by trade name, trademark, manufacturer, or otherwise, does not necessarily constitute or imply its endorsement, recommendation, or favoring by the United States Government or any agency thereof. The views and opinions of authors expressed herein do not necessarily state or reflect those of the United States Government or any agency thereof.

## NOTICE

This report has been reproduced from the best available copy.  
Available in paper copy and microfiche.

Number of pages in this report: 48

DOE and DOE contractors can obtain copies of this report from:

Office of Scientific and Technical Information  
P.O. Box 62  
Oak Ridge, TN 37831;  
(615) 576-8401.

This report is publicly available from the:

National Technical Information Service  
Department of Commerce  
5285 Port Royal Road  
Springfield, Virginia 22161  
(703) 487-4650

## **DISCLAIMER**

**Portions of this document may be illegible in electronic image products. Images are produced from the best available original document.**

## $\beta$ Limit Disruptions in the TFTR Tokamak

E. D. Fredrickson, K. McGuire, A. Janos, M. Bell, R. V. Budny, C. E. Bush,  
J. Manickam, H. Mynick, R. Nazikian, G. Taylor

*Plasma Physics Laboratory, Princeton University*

*P.O. Box 451*

Princeton, New Jersey, 08540 USA

Z. Chang

*University of Wisconsin,*

Madison, Wisconsin

### Abstract

A disruptive  $\beta$  limit ( $\beta$  = plasma pressure/magnetic pressure) is observed in high performance plasmas in TFTR. The MHD character of these disruptions differs substantially from the disruptions in high density plasmas (density limit disruptions) on TFTR. The high  $\beta$  disruptions can occur with less than a millisecond warning in the form of a fast growing precursor. The precursor appears to be an external kink or internal  $(m,n)=(1,1)$  kink strongly coupled through finite  $\beta$  effects and toroidal terms to higher  $m$  components. It does not have the 'cold bubble' structure found in density limit disruptions. There is also no evidence for a change in the internal inductance, i.e., a major reconnection of the flux, at the time of the thermal quench.

## Introduction

The need to withstand major disruptions on ITER and other future tokamak reactors imposes serious design constraints and contributes greatly to the cost of building and operating a large tokamak. In this paper, detailed experimental observations on the high  $\beta$  ( $\beta$  = plasma pressure/magnetic pressure), high temperature disruptions observed on the Tokamak Fusion Test Reactor (TFTR) [1-4] are presented and comparisons made to disruptions in high density plasmas. Since they occur in plasmas with reactor relevant parameters, these observations are of particular interest when discussing disruption control or avoidance in tokamak reactors. The disruptions in high  $\beta$  plasmas, possibly because of the high electron temperatures (with magnetic Reynolds number  $S > 10^9$ ), differ considerably from the disruptions in colder plasmas [5]. Unlike disruptions in high density plasmas, the high  $\beta$  disruptions occur with virtually no warning (e.g., there is no change in the equilibrium plasma equivalent to the collapse of the edge electron temperature in high density plasmas). The growth rates for the precursor MHD activity, when it exists, are sufficiently large that active feedback on MHD activity would not be useful as a method of controlling such disruptions on TFTR and likely in tokamak reactors as well. TFTR is a circular cross-section tokamak and it might be suspected that the physics of the disruptions would differ in 'D' shaped or diverted tokamaks; However similar studies on the noncircular cross-section PDX found many similarities with the disruptions discussed below [6]. Likewise, the observations of fast  $\beta$  collapses reported on JT-60U appear to be similar to those made on TFTR [7].

Most high  $\beta$  disruptions can be avoided by operating TFTR below roughly 90% of the empirically determined  $\beta$  limit (which is in rough correspondence with the  $n=1$  ideal-MHD mode  $\beta$  limit [3]). The limits on  $\beta_n$  ( $=\beta_T/[I(MA)/a(m)B(T)]$ ) and  $\beta_{pol}$  (= plasma pressure/poloidal magnetic field pressure) have been determined empirically (and are in reasonable agreement with the theoretical calculations of the high  $n$  ballooning or external kink limits). For  $q(a)<6-7$ , the limit is approximately  $\beta_n=2$ ; for  $q(a)>6-7$ , the increased peakedness of the profiles changes the stability limit to  $\beta_n<2$ . The maximum attained confinement time in supershot plasmas is found to be nearly independent of beam power and plasma current. Thus, the expected stored energy or normalized beta,  $\beta_n$  can be estimated *a priori*[8,9] making it possible to avoid most  $\beta$ -limit disruptions. In the 1992 run period there were only four major disruptions of high performance supershots out of a total of 550 supershot plasmas.

The high  $\beta_{p01}$  current rampdown experiments are an exception to the above statements in that the disruption rates are relatively high and the empirical  $\beta$  limits are considerably higher than those discussed above. In these experiments, the current profile is strongly modified by the current ramp; this has a large impact on the experimental (and theoretical)  $\beta$  limits. The disruption frequency in these experiments is considerably higher than the frequency for 'normal' supershot operation. This is partly due to less experience in this operating regime resulting in more uncertainty in predicting machine performance; hence the  $\beta$  limits are more often exceeded and control of the very high  $\beta$  plasmas is more difficult. Nevertheless, the disruptions in these plasmas are not significantly different from the high  $\beta$  supershot disruptions discussed here.

A brief descriptive summary of high density plasma disruptions will be given in Section I of this paper, followed by a detailed phenomenological description of disruptions in high  $\beta$ , high temperature plasmas in Section II. It will be shown that there is very little similarity between the two types of disruptions. High  $\beta$  minor disruptions and their similarities to major disruptions will be discussed in Section III. Finally in Section IV some speculations on possible disruption mechanisms and the importance of these observations for future reactors will be discussed.

## I High Density Disruptions

This section provides a phenomenological discussion of density limit disruptions on TFTR. Additional details of studies of high density disruptions on TFTR have already been published [5]. The observations reported here are very similar to those reported on for the JET high density disruptions[10]. Density limit disruptions, for the purpose of this discussion, refer to disruptions which result from the collapse of the electron temperature profile in the manner shown in figure 1. The collapse may be due to radiation from too high a density, as in this case, or it may be due to an influx of impurities or from very strong MHD activity that destroys the flux surfaces and allows large radial transport of heat to the limiter or divertor. These disruptions proceed in three phases. The first phase is the collapse of the electron temperature from the edge, either due to radiation or MHD activity. A sequence of electron temperature profiles leading up to a major disruption is shown in figure 1. As the edge cools, the temperature gradient in the confinement region remains nearly constant, suggesting that there is very little enhancement in the transport co-efficients in this region. As the temperature

profile is contracting, it is also usually the case that in the plasma core the electron temperature becomes very flat (the core region is probably the region within the  $q=1$  surface). If this flatness of the electron temperature profile were ascribed to a stochastic magnetic field geometry, this would tend to suggest that the magnetic shear in this region was small, i.e., the current profile is very flat. Subsequent events, as will be seen, support this conjecture. The collapse continues until the temperature profile resembles a 'tophat' shape, and the cold mantle has extended in to about the  $q=2$  surface. This process typically occurs over a period of several hundred msec. It is during this period that attempts at intervention are most likely to succeed.

When the cold mantle has extended into the region between the  $q=2$  and  $q=1$  surfaces the second phase of the disruption begins, the thermal quench phase. At this point an  $m=1, n=1$  external kink becomes unstable [5]. The mode is classified as an external kink since the 'edge' of the plasma is now quite close to the  $q=1$  rational surface and the plasma is strongly detached from the limiter. The mode mixes cold plasma from the mantle region with the hotter plasma from the core, initiating the second phase of the disruption, the thermal quench. It is at this time that the internal inductance decreases, and a positive spike in the total current is seen. The plasma usually recovers transiently following this event and may persist for of order 10msec before the final thermal quench occurs. Following this, the core plasma temperature is probably below 100eV and the current quench phase begins. No studies have been done on TFTR to address issues of whether impurity influx during the current quench phase plays an important role in keeping the electron temperature low or whether the plasma is stochastic enough at this point that reheat is not possible.

The identification of the disruption precursor mode as having  $m=1, n=1$  is based on electron temperature profile data from two grating polychromators (GPC's) toroidally separated by  $126^\circ$  and on a horizontally viewing soft x-ray camera at the same toroidal location as one of the GPC's. The soft x-ray and electron temperature profiles, along with a schematic of the inferred cold-bubble evolution, are shown in Figure 2. The hollow temperature profile, together with the up-down asymmetric soft x-ray emissivity profile at the same toroidal location is sufficient information to deduce the  $m=1$  cold bubble structure of the mode. The  $n$  number is inferred from the assumption that the rotational transform must be of order unity at this point; the mean free path of an electron is of order 50-100 toroidal transits, so that the electron temperature must be nearly constant on a flux surface. The

growth time of the mode is of order several hundred  $\mu\text{sec}$ . The kink has the topology of a 'cold bubble' which implies very small magnetic shear in the core [5,11,12]. Similar observations of a cold bubble structure were reported in disruption studies on JET [13], but the limitations of two camera x-ray tomography precluded unambiguous identification of the cold bubble [14]. The mode grows and reconnects across the core of the plasma.

In summary, disruptions at high density on TFTR give a relatively early warning during the phase I collapse of the electron temperature profile. During this time low  $m$  MHD activity may also play a role in the temperature profile collapse. The actual current disruption precursor is an external (1,1) kink with a cold bubble topology that grows on a millisecond time scale. The thermal quench phase begins with a reconnection of the magnetic flux within the core region resulting in a fast drop in the plasma internal inductance and concomitant voltage and current spikes.

## II Disruptions in high $\beta$ plasmas

Disruptions at high  $\beta$  in TFTR also have several distinct phases, often beginning with the growth of a precursor, followed by the thermal quench and then the current quench. Unlike disruptions in high density, cold plasmas, there is very little warning; the precursor can have a growth time of less than 50  $\mu\text{sec}$  ( $\gamma = 2 \times 10^4/\text{sec}$ ) and may only be visible for less than 1 msec before the thermal quench. In many cases there was no detectable precursor on the soft x-ray cameras, the Mirnov coils or a single GPC (the operating experience with two GPC's is still rather limited). The thermal quench takes from one to several hundred  $\mu\text{sec}$  during which time the electron temperature drops to less than 100eV which causes the termination of the plasma. Following the thermal quench, the current decay phase begins. There is no evidence for large scale internal redistribution of the current as in high density disruptions.

Fast  $\beta$  collapses (herein referred to as minor disruptions) which resemble in many ways the major disruptions are also observed. The phenomenology of the precursor activity for major and minor disruptions is very similar suggesting a common cause or mechanism is responsible for both; the only significant difference between minor disruptions and major disruptions is that the minor disruption did not have a severe enough impact on the plasma to result in a current quench. The weakest minor disruptions may result in a drop in the central electron temperature of  $< 5\%$  on a time scale of a few msec or less and have little

direct effect on the stored energy. However, minor disruptions are nearly always followed by low  $m$  MHD activity which results in L-mode or lower levels of performance.

Minor disruptions have some superficial resemblance to sawteeth. Both sawteeth and minor disruptions result in a relatively fast drop in the central electron temperature and density, both can affect the neutron rate and both can cause bursts of  $H_{\alpha}$  emission. However, when studied in detail they are clearly different phenomena. The minor disruption precursor is an external kink, similar to that seen for the high  $\beta$  major disruptions, the sawtooth precursor is a tearing-type mode which results in an  $m=1, n=1$  island. The sawtooth leaves the temperature profile flat or slightly hollow inside the reconnection radius (which is somewhat larger than the  $q=1$  radius). The electron temperature profile following a minor disruption is still peaked. The electron temperature either drops over the whole profile or has an inversion radius which is considerably larger than the  $q=1$  radius. The burst of  $H_{\alpha}$  emission occasionally seen following a sawtooth crash occurs when the sawtooth induced heat pulse reaches the limiter, typically 10-20 msec later. The 'heat pulse' following the minor disruption (and the  $H_{\alpha}$  burst) reaches the limiter on a much faster timescale, typically in less than 100  $\mu$ sec. The subsequent appearance of MHD instabilities suggests that there may have been some modification of the current profile as well during the minor disruption. Some examples of minor disruptions will be discussed in more detail in Section III.

The major disruptions (at high  $\beta$ ) are always preceded by a non-thermal burst of ECE emission. This burst may precede the thermal quench phase by up to 100  $\mu$ sec and may signal the onset of global stochasticity, i.e., weakly stochastic fields may allow the escape of energetic electrons before the thermal electron confinement is seriously affected. The non-thermal ECE burst is sometimes preceded by a small increase in the  $H_{\alpha}$  or  $D_{\alpha}$  emission levels. This rise may reflect the initial flux of fast electrons leaking from the plasma and striking the walls, loss of fast ions or possibly a helical distortion of the plasma edge. The thermal quench phase lasts for 100-400  $\mu$ sec.

### Precursor Activity

A relatively large percentage of TFTR disruptions are caught by the disruption trigger system; however the disruption rate is low in supershot plasmas (<1%) and there are only about 20 high  $\beta$  supershot type disruptions for which fast electron temperature, Mirnov and soft x-ray camera data are available. Based on

this limited sample, approximately one half of the high  $\beta$  major disruptions on TFTR are preceded by an observable strong external kink-like mode. There is a tendency for the lower  $q(a)$  plasmas [ $q(a) < 5$ ] to have weaker  $n=1$  precursor activity. However, even in the lowest current, high  $q(a)$  supershot disruptions, there are examples with no detectable precursor activity. For a relatively few disruptions, particularly those at higher current or lower edge  $q$ , a localized, fast growing moderate  $n$  ballooning mode was observed before the disruption. This type of precursor activity will be discussed in a later section.

An example of a disruption with a strong  $n=1$  precursor is shown in Figures 3a and b. In Figure 3a the central electron temperature and the disruption precursor as measured with a Mirnov coil are shown. The Mirnov signal has been numerically integrated (to give the fluctuation amplitude in Gauss) and high-pass filtered (to more clearly show the mode). The initial thermal quench is followed by a brief period of reheating due to NBI injection. In Figure 3b the electron temperature profiles are shown up to the non-thermal burst of ECE emission. The precursor structure is easily visible on the temperature data. High  $\beta$  disruptions with a very weak or undetectable precursor appear otherwise similar; an example is shown in Figures 4a and b. The Mirnov data has been treated in the same manner as that in Figure 3a and is displayed on the same vertical scale. No precursor activity is visible either in the Mirnov data, or in the fast temperature data shown in Figure 4b.

The type of precursor MHD activity seen before minor and major disruptions is only observed before disruptions; sawtooth precursors are considerably different. The most important difference between sawtooth and high  $\beta$  disruption precursors is that the sawtooth precursor results in a poloidally and radially localized flattening of the electron temperature, suggesting the presence of an island (Fig. 5). In contrast, the disruption precursor only displaces the plasma, but does not create flattened regions (Fig. 6). The implication is that the disruption precursor is predominantly an ideal mode while the sawtooth precursor has more of a resistive nature. The growth rates for the two instabilities can be similar, however.

The disruption precursor is much more strongly coupled to higher  $m$  modes than are sawtooth precursors. This can be seen by comparing the radial displacement of the flux surface,  $\xi(r)$  for a precursor to a major disruption (Fig. 7) to the  $\xi(r)$  for a sawtooth precursor (Fig. 8). The  $\xi(r)$  is determined from contour plots (such as is shown in Figure 9) with the assumption that  $T_e$  is constant on a flux

surface. The sawtooth precursor even in relatively high  $\beta_{pol}$  plasmas causes comparatively little displacement of the flux surfaces beyond the  $q=1$  surface, and only on the outboard side of the plasma. The disruption precursor has much stronger poloidal coupling of the internal (1,1) mode to the higher  $m$ ,  $n=1$  components and the radial displacement is large out to the edge of the plasma. Within the  $q=1$  surface, the sawtooth precursor has a similar displacement on the inboard and outboard sides. In contrast, the disruption precursor is asymmetric within the  $q=1$  surface, presumably reflecting the strong coupling of the even (2,1) mode with the odd (1,1) mode. Since the relative phase is such as to add on the outboard side, the modes will tend to cancel on the inboard side.

The phasing of the coupling of the different  $m$  components is such as to add on the outboard side of the plasma. This can be seen from the lack of phase inversions in the electron temperature fluctuation data, shown in the contour plot of Figure 9. The Mirnov array data shows that near the plasma edge the dominant mode structure is  $m \approx q(a)$ ,  $n=1$  (Fig. 10a). It is not clear from the GPC data whether the mode has a strong ballooning character; however the data from the Mirnov system shows that the magnetic fluctuation level is roughly ten times larger on the outboard midplane than on the inboard midplane (Fig. 10b). In contrast to low  $m$  MHD activity such as tearing modes [15], the displacement of the flux surfaces is quite large over most of the plasma minor radius.

The internal poloidal structure of the precursor cannot be determined with present diagnostics due to limited resolution in the poloidal direction. The vertically viewing soft x-ray camera has chords tangent at the same radial (and toroidal) locations as the horizontally viewing grating polychromator (GPC). Typically the fluctuations in the chord integrated soft x-ray emission are dominated by the local fluctuations at the hottest, densest part of the chord integral due to the strong peaking of the soft x-ray emissivity. However, for some high  $\beta_{pol}$  disruptions the local temperature fluctuations measured with the GPC and the vertical chord integrated soft x-ray emission are out-of-phase on the outboard side of the plasma. These observations suggest strong coupling of an  $m=1$  to higher  $m$ 's resulting in strong distortions of the flux surface to the edge of the plasma.

Figure 11 shows the relative phase of the local electron temperature fluctuations *versus* minor radius and the relative phase of the chord integrated soft x-ray fluctuations *versus* the minor radius of the tangency point. In this case the chord integrated soft x-ray emissivity fluctuations are  $180^\circ$  out of phase with the local electron temperature fluctuations. The dominant component of the soft x-ray

fluctuations comes from changes in the chord integral due to distortions of the flux surfaces, rather than from changes in the emissivity at the hottest, densest part of the chord. This explanation is also consistent with the relatively small chord integral soft x-ray fluctuation level compared to the local temperature fluctuation level at minor radii around  $r/a = 0.5$ . In Figure 12 are shown the fluctuation amplitudes for the vertically viewing soft x-ray camera and the local temperature fluctuation measurements. The amplitude of the soft x-ray fluctuations peaks at a much smaller tangency radius ( $r/a \approx 0.1$ ) than the local electron temperature fluctuations ( $r/a = 0.5$ ). For both signals the phase is relatively constant on the outboard side of the plasma and there is a jump of about  $180^\circ$  across the center of the plasma where the  $m=1$  component is dominant. On the inboard side there is an additional phase jump corresponding to the point where the  $m=2$  component becomes dominant.

The coupling of the (1,1) mode to higher  $m$  modes is weaker in higher current, lower  $\beta_{pol}$  plasmas. In Figure 13 is shown the flux surface displacement for a high  $\beta$  disruption at 2.5MA (to be compared to the displacement from a 1 MA disruption precursor shown in figure 7). In this case the quickly growing precursor does not show as strong of an 'external' character as is present in the more slowly growing precursor and the displacement is roughly half of that in the lower current case. Although the coupling is weaker, this mode is still far more 'external' than the typical sawtooth precursors. Part of the difference here might be attributed to the lower edge  $q$  in the case with the weaker precursor.

The characteristics of the disruptions which lack detectable precursors appear similar in other respects to those of disruptions with precursors. This suggests that the lack of detectable precursors of the type seen in Figure 3 on some disruptions suggest that the growth rate for the disruption precursor is in some cases very large. The growth time for the disruption precursors were studied for a wide variety of shots and were found to vary from less than 50  $\mu$ sec to greater than 10 msec. The disruption precursor may also show the non-linear growth that has previously been seen for sawtooth precursors, i.e., a relatively long phase of slow growth followed by a short period of much more rapid growth. In Figure 14 is shown the mode amplitude as measured with a Mirnov coil vs time before the disruption. Fitted to the data is a curve representing an early exponential growth rate of 400 Hz followed by a growth rate of 2 kHz in the final 1 msec prior to the thermal quench. It is quite possible that growth rates in excess of  $2 \times 10^4$ /sec would not be detectable due to the digitizing rates of typically 100kHz and the plasma

rotation rates which may be less than 1kHz. Thus cases where no precursor activity was observed may have had precursors with growth rates in excess of  $2 \times 10^4$ /sec. This growth rate is much faster than the Sweet-Parker [ $\tau_{S-P} = (\tau_R \tau_{\text{Alfvén}})^{1/2} \approx 8 \text{msec}$ ] or tearing mode growth rates ( $\tau_{\text{tearing}} = \tau_R^{3/5} \tau_{\text{Alfvén}}^{2/5} \approx 60 \text{msec}$ ), but slower than an ideal growth rate ( $\tau_{\text{Alfvén}} = R/V_{\text{Alfvén}} \approx 0.3 \mu\text{sec}$ ,  $\tau_R = 4\pi a^2/\eta c^2 \approx 200 \text{sec}$ ). However, for very hot (collisionless) plasmas, the inertia of the plasma plays a more important role than the resistivity. In this case the layer width is approximately  $c/\omega_{pe}$  ( $\omega_{pe}^2 = 4\pi n_e^2/m_e$ ,  $c/\omega_{pe} \approx 7 \times 10^{-4} \text{m}$ ), and the growth rate is given approximately by  $\gamma \tau_{\text{Alfvén}} = q'\rho_s/q$  or  $\gamma^{-1} \approx 30 \mu\text{sec}$  [16-18].

The radial structure of the major disruption precursors suggests that the precursor is at least partially an external kink. However, there is no experimental evidence to suggest that wall stabilization has affected either the precursor growth rate or the observed disruptive  $\beta$  limit. Experiments at high  $\beta$  have been carried out in TFTR at major radii ranging from 2.45m to 2.62m. For the smaller major radius, the average radius of the vacuum vessel,  $r_{\text{vac}}$ , is approximately  $1.4a_p$  where  $a_p$  is the plasma minor radius. However, the plasma is not centered in the vacuum vessel, being much closer to the wall on the inboard side. Thus, the effective radius of the vacuum vessel with respect to stabilization of modes with a ballooning structure is probably closer to  $1.6a_p$ . For the larger major radius the vacuum vessel forms a rather close fitting, nearly concentric shell with  $r_{\text{vac}} \approx 1.2a_p$ . Typical rotation rates are much faster than the resistive skin time of the vacuum vessel, thus the vacuum vessel can be considered to be an ideal conducting shell. There is no observed difference in the growth rates or thermal quench times between disruptions at small or large radii, i.e., between disruptions with 'close' or with 'loose' fitting conducting shells. This is consistent, however, with PEST calculations which suggest that the conducting wall does not strongly affect stability in the case of peaked pressure profiles[19].

### Non-thermal ECE emission

All major high  $\beta$  disruptions have a burst of non-thermal ECE less than 100  $\mu\text{sec}$  before the thermal quench. The emission is broad-band and can have an effective temperature greater than 50keV. The burst of non-thermal ECE emission almost certainly reflects the presence of a very energetic, non-thermal electron population, possibly in the plasma edge, similar to the explanation given for the non-thermal bursts often observed during ELM's [20,21]. The origin of this population is not clear. This population may have been generated near the time of

the disruption, possibly as a result of local tearing of the flux surfaces driven by the kink instability, or was a population well confined in the plasma core, then released at the time of the disruption or possibly represents a velocity space instability where many fast tail electrons are scattered perpendicular. Either explanation has difficulties, however. While there were very likely runaways present during the ohmic target phase of the discharge, during NBI the plasma density rises and the loop voltage drops nearly to zero due to beam and bootstrap driven currents, thus it does not seem likely that a runaway population could exist for more than 100-200 msec [22]. On the other hand, there is no evidence to support the existence of a strong reconnection of the flux at the time of the disruption, thus there are no strong electric fields which might generate the runaways.

### Thermal quench

The thermal quench phase generally starts less than 1msec after the non-thermal ECE burst. In many cases there is a period of several hundred microseconds during which the electron temperature profile looks very normal, but slightly reduced in amplitude from the time before the non-thermal burst [Fig. 15a and the profiles labeled (a) and (b) in Fig. 15b.]. The transition to the thermal quench phase can then be very abrupt. During the thermal quench no evidence has been found to suggest that the quench begins at the plasma edge (for instance, as if a cold wave of impurities were moving into the plasma), nor that there is flattening near rational surfaces (e.g., as if 2/1 and 3/2 tearing modes were creating a growing stochastic region in the plasma). There is no evidence that islands or stochastic regions form first near low order rational surfaces. The electron temperature profile remains peaked and relatively featureless during the thermal quench (Fig. 15b). Following the thermal quench, the electron temperature is probably less than 50-100 eV and the current quench phase begins. In contrast to disruptions at high density, it does not appear that there is a flux reconnection, with the concomitant changes in  $l_i$  and the negative voltage spike, preceding the current quench.

There are no direct measurements of the ion temperature on a relevant timescale for disruption studies. However, neutron scintillators provide a measurement of the neutron flux on a fast timescale. These detectors typically show a drop in the neutron emission of about 25% in 100  $\mu$ sec at the time of the non-thermal ECE burst (Fig. 16). In this figure there is a relatively slow drop in the neutron emission rate over a period of about 0.5 msec before the non-thermal ECE

burst, coupled with a slow rise in the  $H_{\alpha}$  emission. This may represent a small loss of the fast ion population. The neutron rate then remains roughly constant for 1 - 2 msec followed by a fairly rapid drop. It is not clear at this time which of the neutron rate drops reflects a change in the thermal ion temperature and which is related to the fast ion population. However, as the thermal neutron rate is typically less than about 30% of the total rate, it would be reasonable to ascribe the initial 25% drop to a rapid decrease in the ion temperature and the later drop to a loss of the fast ion tail.

### Current quench

Unlike disruptions in colder, lower  $\beta$  plasmas, there is no clear evidence for a reconnection of the magnetic flux in high  $\beta$  disruptions. However, interpretation of the magnetics data on a submillisecond timescale during high  $\beta$  disruptions is difficult. There appears to be a rapid loss of stored energy in a period of a few hundred  $\mu$ sec. As the vertical feedback system responds on a much slower timescale, the energy loss results in a large, fast inward shift of the plasma, making the determination of  $\beta$  and  $l_i$  very difficult. The positive current spike observed in high  $\beta$  disruptions is much weaker than in high density disruptions. The current spike is most probably due to the inward shift of the plasma following the thermal quench.

### III Minor Disruptions

Minor disruptions have many of the same features as the high  $\beta$  major disruptions, suggesting that they are a less severe manifestation of the MHD instability responsible for the high  $\beta$  major disruption. The minor disruptions initially cause a drop in the central electron temperature of similar magnitude to that of a sawtooth; however the electron temperature is generally still peaked afterward and there is usually no inversion. The most notable difference between the minor and major disruptions is that the minor disruptions often lack the very strong non-thermal burst of ECE. In the cases where this burst is present, it is typically limited to frequencies which map to the outer edge of the plasma. The range of precursor activity seen before the minor disruptions is very similar to that observed before major disruptions, i.e., anything from large kink-like modes to very weak or undetectable precursors.

In figures 17 and 18, the electron temperature profile before and after a minor disruption are shown. The two minor disruptions discussed here were

chosen in that their effect on the electron temperature was similar and relatively small; in both cases the drop in the central electron temperature is about 0.5keV or comparable to that of a sawtooth. However, the precursor was much stronger in the first case than in the second and these two minor disruptions had a considerably different effect on the total stored energy and on the neutron rate, suggesting that either the thermal or the fast ion population was affected differently in the two cases. In the first case the neutron rate dropped by about 20% over a period of 4 msec, the diamagnetic  $\beta$  dropped by about 10% and the plasma column shifted inwards in major radius by about 4 cm (Figs. 17 and 19), all indicating that there was a substantial loss of kinetic energy in the plasma. In the second case the drop in the neutron rate was of order 5%, the change in the stored energy was smaller and there was very little shift in the plasma position, evidenced by magnetics measurements, the electron temperature profile and by the lack of a strong burst of  $H_{\alpha}$  (Figs. 18 and 20).

Ion temperature measurements are not fast enough to resolve the question of whether the neutron drop is due to ion cooling or loss of fast ions[23]. On a 100 msec timescale, the effect of the minor disruption on the thermal ions was very similar in both cases; the central ion temperature dropped from about 25 keV to about 15 keV. An explanation is that fast ions (responsible for typically 30-50% of the neutron production) are lost from the plasma during the disruption in the first case.

The TFTR minor disruptions have many of the same features as the JET X-events, i.e., a rapid drop in stored energy, central electron temperature and neutron rate coupled with a spike in the edge  $H_{\alpha}$  emission[24]. Unlike the x-events in JET which were often attributed to impurity influxes, the minor disruptions in TFTR are clearly an MHD event which then reduces the plasma  $\beta$ , resulting in the vertical field transiently moving the plasma into the inboard limiter, heating the limiter and leading to an increase in recycling.

#### IV Discussion

While the disruption precursor appears to be an ideal, pressure driven kink mode, the trigger mechanism for the mode is not understood. Typically, in supershot plasmas similar to these that have disrupted, the  $q$  on axis is measured to be below unity[25] and most stability codes predict that the  $n=1$  ideal mode is unstable[26,27]. It remains an unanswered question as to what mechanism is stabilizing the ideal mode under normal operational conditions and why it suddenly

becomes unstable in the cases which disrupt. Curiously, while fishbone-like (1,1) bursting modes (or other low m,n modes) are commonly observed in supershots[28], they are not usually observed in plasmas that disrupt. A second problem is in developing a model by which an apparently ideal mode can cause a sudden, catastrophic loss of confinement. The disruption precursor shows no evidence for the formation of islands; it appears to be predominantly an ideal instability. If the thermal quench were due to global stochastization of the magnetic field, extensive tearing of the field lines must occur in a very hot (5-10 keV) plasma in a very short (100 $\mu$ sec) time.

The thermal quench is not apparently accompanied by a reconnection of the helical flux, which in the case of density limit disruptions leads to a positive current spike and a drop in  $l_i$ . The evolution of the electron temperature profile is also not consistent with a global reconnection of the magnetic flux, remaining peaked at all times. Given the lack of global reconnection, the enhancement in transport during major and minor disruptions must be attributed to local stochasticity. The amount of enhancement required may be estimated from the ratio of the thermal confinement time to the thermal quench time and is about three orders of magnitude. This may be due to fine scale reconnection of the field lines near rational surfaces driven by micro-tearing or ballooning modes. This might superficially explain the non-thermal burst of ECE observed at major and sometimes during minor disruptions. As the run-aways would be more sensitive to weakly stochastic magnetic fields, it might be expected that they would be lost first, consistent with the ECE burst being observed prior to the thermal quench.

### **Ballooning assisted tearing**

New experimental evidence suggests an intriguing model that the presence of an ideal (or resistive) mode, at or near the ballooning stability threshold might provide the trigger for the disruption. In this case, the distortions to the plasma caused by a large ideal mode might locally push the plasma over the ballooning mode stability boundary. A ballooning mode would then form locally, possibly eventually breaking the flux surfaces and resulting in large enhancements in transport[29-31]. Ballooning modes of this type are often observed in non-disruptive TFTR supershot plasmas at high  $\beta$  and in high  $\beta$  plasmas created with current rampdowns[32]. As the structure of the ballooning mode in the model proposed above is both toroidally and poloidally localized, it is very difficult to rule

this model out based on observations at one toroidal location. Several examples have been found, however which suggest that this type of disruption may be relatively common, particularly at higher currents. In Figure 21 a ballooning precursor to the disruption was captured in the fast window on two grating polychromators separated toroidally by 126 degrees. The suspected ballooning mode is marked and appears first on GPC2 at 3.95146 sec and later on GPC1 at 3.95152 sec with larger amplitude. From this data it is possible to deduce that the ballooning mode is localized within a toroidal angle of about 45° on the outboard midplane. As the ballooning mode is localized to the region where the n=1 mode displaces the plasma outwards on the outboard midplane, it is reasonable to assume that it has no real frequency in the plasma frame and the toroidal mode number n of the ballooning mode is just the ratio of the frequency of the ballooning mode to the n=1 mode, thus,  $n \approx 10$ . The magnitude of the displacement approximately triples in 80  $\mu$ sec, giving a growth rate of  $\gamma \approx 1.2 \times 10^4/\text{sec}$ .

A second example of a ballooning precursor to a disruption is shown in Figure 22. In the previous example, both the ballooning mode and the n=1 mode were present prior to the disruption, in this case there was no visible n=1 mode. There was an (m,n) = (4,3) mode present, a mode which does not have a previous association with disruptions. It is interesting to note that the ballooning bursts only occur on every third (4,3) oscillation, as would be expected for a strongly toroidally localized mode. This example provides some evidence that the ballooning mode alone could be responsible for the high  $\beta$  disruptions.

### Stochastic ion orbits

The rather large deformations of the plasma caused by the ideal mode may result in stochastic orbits for the fast ions, even before the magnetic field geometry becomes stochastic, resulting in loss of some fraction of the fast ion population. This could occur as the fast ions do not exactly follow the field lines, but that they deviate from the flux surfaces due to various drifts. In Figure 7 are shown the very approximate stochastic thresholds for 100 keV deuterium ions (the beam injection energy is about 100 keV) compared to the experimentally measured displacement of the flux surface. The stochastic threshold for an n=1 perturbation for passing fast ions used here is given approximately by [33]

$$\xi_r > r / (4\rho_{\text{fast}} q' q^2)$$

and for the trapped fast ions is [34,35]

$$\xi_r > R / [\rho_{\text{fast}} q' (\pi q / \epsilon)^{3/2}].$$

Both the passing and trapped thresholds are shown in figure 7. While these estimates are uncertain, they suggest that even an ideal kink mode with amplitudes similar to that which are measured could result in significant fast ion losses through stochastization of their orbits. This could explain the early, slow drop in neutron rate seen in major and minor disruptions with strong precursors and may also be partially responsible for the drop in stored energy and early rise in the H $\alpha$  recycling light. The loss of fast ions would tend to charge the plasma, and in this example, drop the rotation rate and mode frequency. This may explain the measured change in the mode frequency (c.f. Fig. 19). Of the drop in neutron rate seen in figure 19 of about 20%, one half or 10% can be ascribed to the effect the drop in central density of about 20% would have on beam-target reactions leaving 10% unexplained. If the remaining 10% were due to stochastic losses of fast ions, it would be necessary to lose all of the fast ions outside  $r=0.45m$ . As most of the beam ions within  $r=0.55m$  are passing, the stochastic threshold for passing ions would have to be about one half of the estimate shown in figure 7.

The implications of this model for the design of ITER or other reactors are ominous. ITER will have a relatively large fast ion component. In the expressions for the stochastic thresholds, scaling to ITER is in the dimensionless parameter  $\rho_{fast}/a$  which is very similar for the TFTR beam ions and the ITER alphas. If a significant fraction of the fast ion (alpha) population in ITER is lost on a time scale of msec by this process, the energy will probably not go to the divertor as is presently expected for disruptions, but could end up on the first wall.

### Summary

The most commonly observed precursor activity to high  $\beta$  disruptions on TFTR is an  $m=1, n=1$  internal kink strongly coupled to higher  $m$  kink modes. The precursor can have a growth rate greater than  $10^3/\text{sec}$ . The precursor appears to be ideal in that there is no evidence for island formation or the growth of stochastic regions. The actual transport mechanism responsible for the thermal quench during the disruption is not clear at this point. The destruction of the flux surfaces may be due to the growth of local ballooning modes. Some of the heat transport may also occur through loss of energetic ions through a stochastic orbit mechanism. There is no evidence that decreasing the plasma wall separation (to as low as  $r_{vac}=1.2a_p$ ) affects the mode growth rate, achievable  $\beta$ , or rate of thermal quench.

The high  $\beta$  disruptions in high temperature plasmas ( $S > 10^9$ ) studied on TFTR will present more challenging problems for future tokamak reactors than high density disruptions. The high  $\beta$  disruptions can occur with very weak or no identifiable precursors that will make direct feedback on MHD instabilities unfeasible. The high  $\beta$  disruptions occur without warning in the form of edge temperature collapses, increases in radiation, etc., making disruption avoidance based on global plasma parameters very difficult. On the basis of TFTR experience, the best disruption avoidance approach would be to refine the understanding (empirically and theoretically) of the disruptive  $\beta$  limit. However, given the uncertainty in this limit, based on global parameters, it may be necessary to operate a machine like ITER at less than 80% of the limit to achieve an acceptably low disruption rate. This would reduce the maximum performance of ITER in terms of power generation by up to 40%.

#### Acknowledgments

We would like to thank Drs. K. Young and R. Hawryluk and the TFTR group for supporting these experiments. Supported by the U.S. Department of Energy Contract Number DE-AC02-76CH03073.

## Bibliography

- [1] K. M. McGuire and the TFTR Group in Plasma Physics and Controlled Nuclear Fusion Research 1986 (Proc. 11th Int. Conf. Kyoto, 1986), Vienna (1987) Vol.I, 421.
- [2] A. W. Morris, E. D. Fredrickson, K. M. McGuire, M. G. Bell, M. S. Chance, R. J. Goldston, R. Kaita, J. Manickam, S. S. Medley, N. Pomphrey, S.D. Scott, M. C. Zarnstorff in Proc. of the 14th European Conference on Controlled Fusion and Plasma Physics, Madrid Spain 1987, Vol I, p189.
- [3] J. Manickam et al., in Plasma Physics and Controlled Nuclear Fusion Research 1988 (Proc. 12th Int. Conf. Nice, 1988). Vienna (1989) .
- [4] E. D. Fredrickson and the TFTR Group in Plasma Physics and Controlled Nuclear Fusion Research 1986 (Proc. 13th Int. Conf. Washington, 1990), Vienna (1991) Vol.I, 559.
- [5] Fredrickson, E. D., K M McGuire, M G Bell, C E Bush, R V Budny, A C Janos, D K Mansfield, Y Nagayama, H K Park, J F Schivell, G Taylor, M C Zarnstorff, J F Drake, R Kleva, Nucl. Fusion **33**, 1993.
- [6] G. Jahns, et al. Nucl. Fusion **28** (1988) 881 and Princeton Plasma Physics Laboratory Report #2482, PPPL-2482 (1987).
- [7] S. Ishida, M. Matsuoka, M. Kikuchi, S. Tsuji, T. Nishitani, Y. Koide, T. Ozeki, T. Fujita, H. Nakamura, N. Hosogane, K. Kamada, R. Yoshino, D. Humphreys, N. Isei, M. Sato, H. Hsuan, H. Shirai, T. Hirayama, M. Azumi, H. Kubo, M. Kuriyama, N. Nemoto, H. Takeuchi, JT-60 Team. in Plasma Physics and Controlled Nuclear Fusion Research 1992 (Proc. 14th Int. Conf. Wurtzburg, Germany). Vol. I, IAEA, Vienna (1993) 219.
- [8] M. Bell et al., in Plasma Physics and Controlled Fusion Research 1988 (Proc. 12th Int. Conf. Nice, 1988), Vol. I IAEA, Vienna (1989) 27.
- [9] J. D. Strachan and the TFTR Group, Phys. Rev. Lett. **72** (1994) 3525.
- [10] J A Wesson, R D Gill, M Hugon, et al., Nucl. Fusion **29** (1989) 641.
- [11] B B Kadomtsev, O P Pogutse, Sov. Phys JETP **38** (1974) 283..
- [12] R G Kleva and J F Drake, Phys. Fluids B **3** (1991) 372.
- [13] D J Campbell, P A Duperrex, A W Edwards et al., in Plasma Physics and Controlled Nuclear Fusion Research 1986 (Proc. 11th Int. Conf. Kyoto, 1986), Vol. I, IAEA, Vienna (1987) 433.

- [14] S W Wolfe, A W Edwards, R D Gill, et al., in *Controlled Fusion and Plasma Heating* (Proc. 17th Eur. Conf. Amsterdam, 1990), Vol. 14B Part I European Physical Society (1990) 335.
- [15] Z. Chang et al., accepted for publication in *Nucl Fusion*. (1984).
- [16] J. F. Drake, *Phys. Fluids* **21** 1777 (1978).
- [17] F. Porcelli, *Phys. Rev. Lett.* **66**, 425 (1991).
- [18] L. Zakharov, B. Rogers, S. Migliuolo, *Phys. Fluids* , 2498 (1993).
- [19] J. Manickam (private communication)
- [20] G. Taylor, C. E. Bush, E. D. Fredrickson, H. K. Park, and A. T. Ramsey, *Nucl. Fusion Lett.* **32**, 1867 (1992).
- [21] L. Porte, D. V. Bartlett, D. J. Campbell, and A. E. Costley, in *Proc. of the 18th Eur. Conf. on Controlled Fusion and Plasma Physics* (Berlin, 1991), **15c**, Part IV, European Physical Society 357 (1991).
- [22] G. Taylor, C. W. Barnes, B. J. Braams, A. Cavallo, P. C. Efthimion, C. F. F. Karney, S. Tamor, M. C. Zarnstorff and S. Zweben, in *Proc. of the 16th Eur. Conf. on Controlled Fusion and Plasma Physics* (Venice, 1989), Vol. I, p31.
- [23] M. Bitter, K. W. Hill, S. Cohen, S. von Goeler, H. Hsuan, L. C. Johnson, R. Raftopoulos, M. Reale, N .Schechtman, S. Sesnic, F. Spinou, J. Timberlake, S. Weicher, N. Young, and K. M. Young, *Rev. Sci. Instrum* **57** (1986) 2145.
- [24] A. Gibson and the JET team in *Plasma Physics and Controlled Nuclear Fusion Research 1992* (Proc. 14th Int. Conf. Wurtzburg, Germany). Vol. I, IAEA, Vienna (1993) 99.
- [25] F. Levinton, S. H. Batha, M. Yamada, and M. C. Zarnstorff, *Phys. Fluids B*
- [26] M. H. Hughes , M. W. Phillips, and E. D. Fredrickson, *Phys. Fluids B* **5** 3267 (1993).
- [27] W. Park, D A Monticello, E Fredrickson, and K M McGuire, *Phys. Fluids B* **3** (1991) 507.
- [28] R.Kaita, R. B. White, A. W. Morris, E. D. Fredrickson, K. McGuire, S. S. Medley, and S. D. Scott, *Phys. Fluids B*, **2**, 1584 (1990).
- [29] Y. Nagayama, M. Yamada, S. Sabbagh, E. Fredrickson, et al., *Phys. Fluids B* **5** (1993) 2571.
- [30] M.N. Bussac and R. Pellat, *Phys. Rev. Lett.* **59** (1987) 2650.
- [31] C. C. Hegna and J. D. Callen, *Phys. Fluids B* **4**, 3031 (1992).
- [32] J. Kesner, M. E. Mauel, G. A. Navratil, et al., *Phys. Fluids B* **5**, 2525 (1993).
- [33] H. E. Mynick, *Phys. Fluids B* **5** (1993) 1471.
- [34] R. J. Goldston, R. B. White and A. H. Boozer, *Phys. Rev. Lett.* **47** (1981) 647.

8/19/94

[35] R. B. White and H. E. Mynick, Phys. Fluids B 1 (1989) 980.

## Figure Captions

- Figure 1 Profiles of the electron temperature shown at 40 msec intervals leading up to a major disruption. The temperature becomes very flat within the inferred  $q=1$  surface. The profile at 4.66s is approximately 2msec before the thermal quench.
- Figure 2 Profiles of the electron temperature at 50  $\mu$ sec intervals during the growth of the (1,1) external kink. The hollow  $T_e$  profiles clearly demonstrate the existence of the cold bubble topology as indicated in the cartoon sketches. The up-down asymmetry is inferred from a horizontally viewing soft x-ray camera.
- Figure 3a The central electron temperature and the integrated signal from a Mirnov coil over the 5msec of a major disruption. The 15MW of neutral beam heating remained on until 4.115s, and are probably responsible for the brief reheat following the initial thermal quench from 4.1121 to 4.1125sec. The burst of non-thermal emission from 4.112 to 4.1121sec is arbitrarily clipped in this figure. The Mirnov data is numerically integrated. The mode frequency is dropping before the disruption.
- Figure 3b Profiles of the electron temperature across the midplane up to the non-thermal burst of electron cyclotron emission. The very strong perturbations to the flux surfaces are clearly visible on the outboard side of the plasma. The apparent ballooning nature may be misleading due to lack of measurements on the inboard side.
- Figure 4a Data similar to that in Fig. 3a, but illustrating the absence of a detectable precursor.
- Figure 4b Data similar to that in Fig. 3b. There is no evidence for precursor activity in the electron temperature profile.
- Figure 5 Profiles of the electron temperature vs. major radius at two phases of the sawtooth precursor. The profiles were chosen at times to show the 'island' flat spot on the inboard and the outboard sides of the plasma.

The structure of the precursor is seen to be well confined to be within the  $q=1$  surface.

- Figure 6 Profiles of the electron temperature vs. major radius at two phases of a disruption precursor. The strong external character of the precursor is evident, as is the lack of a flat region in the temperature profile. This suggests that there is no island, but that the mode is ideal.
- Figure 7 The radial displacement of the flux surfaces caused by the precursor 200  $\mu$ sec before the major disruption as determined from the data shown in Fig. 5. Shown for comparison are the approximate theoretical mode amplitude thresholds for stochastic passing and trapped 100 keV Deuterium ions.
- Figure 8 The radial displacement of the flux surfaces caused by a sawtooth precursor in a high  $\beta_{pol}$  plasma. The perturbations from the sawtooth precursor are to first order localized within the  $q=1$  surface, but toroidal and finite  $b$  effects result in measurable displacements on the outboard side of the plasma. The magnetic fluctuation level for the sawtooth precursor was approximately 0.1 Gauss at the plasma edge for the sawtooth precursor and  $>10$  Gauss for the disruption precursor.
- Figure 9 A contour plot of the temperature data shown in Fig. 3a. The displacement of the flux surfaces,  $\xi_r$ , can be measured directly in this plot.
- Figure 10 Phase and amplitude analysis of the Mirnov data showing the  $(m,n)=(6,1)$  structure of the mode at the plasma edge and the strong ballooning nature of the mode. The data from the Mirnov coils has been corrected to compensate for varying separation of the coils from the plasma edge.
- Figure 11 The relative phase of the fast electron temperature and chord integrated soft x-ray emission disruption precursor fluctuations vs. minor radius as seen on the measurement. The soft x-ray and local temperature fluctuations are approximately out-of-phase. The relative

phase changes by approximately  $180^\circ$  across the plasma center, showing that internally the mode has odd  $m$ .

- Figure 12 The amplitude of the chord integrated soft x-ray emission from a vertically viewing soft x-ray camera and local electron temperature fluctuations shown vs. minor radius. The amplitude of the temperature fluctuations peaks at about  $r/a=0.5$  and at  $r/a=0.1$  for the chord integrated soft x-ray fluctuations.
- Figure 13 Comparison of the flux surface displacement 100  $\mu$ sec prior to a disruption with a weak precursor to the flux surface displacement for the precursor shown in Figure 6, but about 3 msec before the disruption at a time when the amplitude was comparable. The scale is chosen to be the same as for figures 6 and 8.
- Figure 14 The amplitude in Gauss of the precursor as seen with a Mirnov coil in the final milliseconds before the major disruption. Note the suggestion of a final growth rate much larger than the initial growth rate.
- Figure 15a Profiles of the electron temperature during the thermal quench phase of a high  $\beta$  disruption. As the quench proceeds, the plasma loses energy and the vertical field pushes the plasma inward. The profile does not collapse from the edge as in the high density disruptions, nor is there evidence for local flattening near rational surfaces.
- Figure 15b Trace of the central electron temperature for the disruption in figure 18a. Following the non-thermal burst of ECE, the plasma is actually stationary for several hundred  $\mu$ secs before the thermal quench begins.
- Figure 16 The central electron temperature, edge poloidal magnetic field fluctuations, fast measurement of the neutron emissivity and the  $H_\alpha$  emissivity through the high  $\beta$  major disruption shown in figure 3.
- Figure 17 Profiles of the electron temperature 10 msec apart before and after a minor disruption with a strong precursor.

Figure 18 Profiles of the electron temperature 1 msec apart before and after a minor disruption with a very weak precursor.

Figure 19 The diamagnetic  $\beta_{pol}$  and the major radius as determined from magnetic measurements through the disruption shown in Figure 17. On a faster timescale are shown the central electron temperature, the neutron source rate and the edge  $H_{\alpha}$  emission during the minor disruption shown in Figure 17. Notice the large increase in  $H_{\alpha}$  emission, and the 30% drop in neutron emission.

Figure 20 The diamagnetic  $\beta_{pol}$  and the major radius as determined from magnetic measurements through the disruption shown in Figure 18. On a faster timescale are shown the central electron temperature, the poloidal magnetic fluctuation level at the plasma edge, the neutron source rate and the edge  $H_{\alpha}$  emission during the minor disruption shown in Figure 16. Notice that there is no measureable change in  $H_{\alpha}$  emission and the neutron source strength drops by only 10%.

Figure 21 Experimental measurements of a toroidally and poloidally localized ballooning mode. The lower frequency  $n=1$  mode breaks the toroidal symmetry and allows the toroidal localization.

Figure 22 Experimental measurements of a toroidally and poloidally localized ballooning mode. The lower frequency (4,3) mode breaks the toroidal symmetry and allows the toroidal localization.

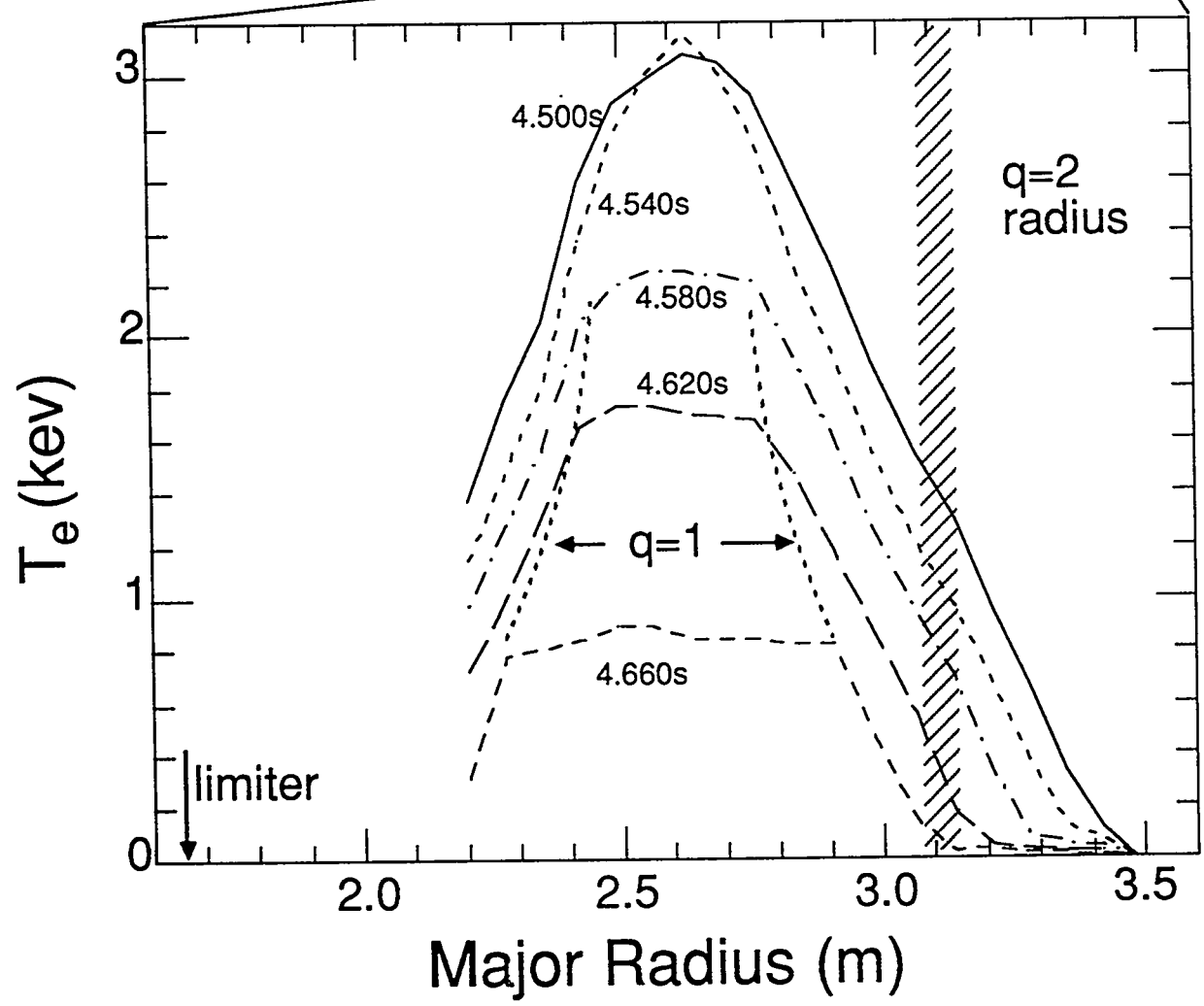
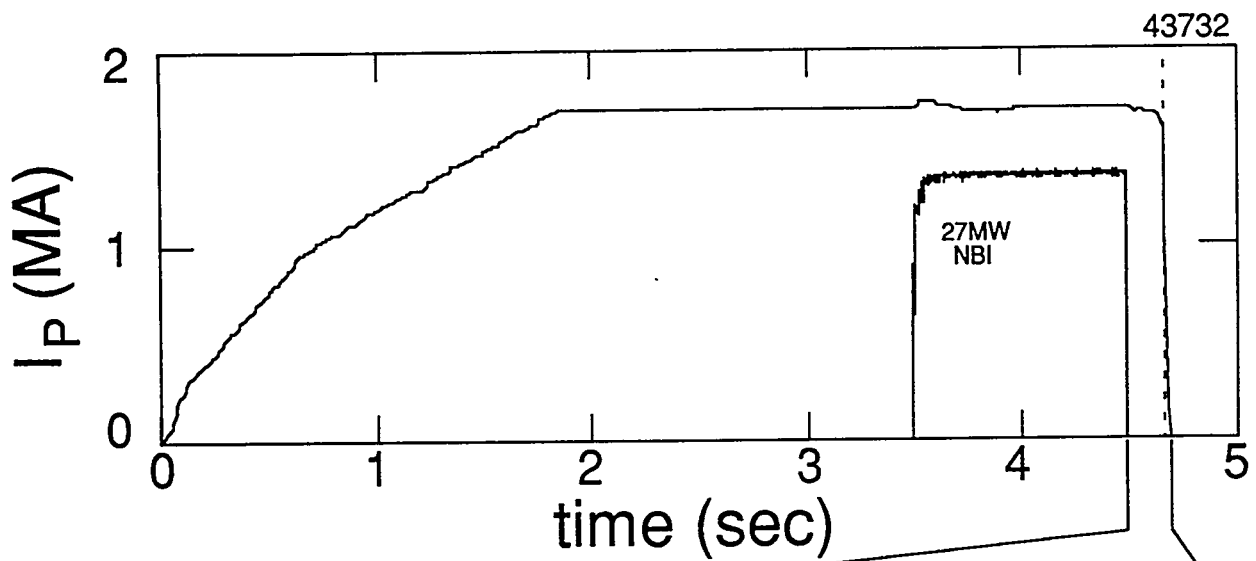


Figure 1

Figure 2

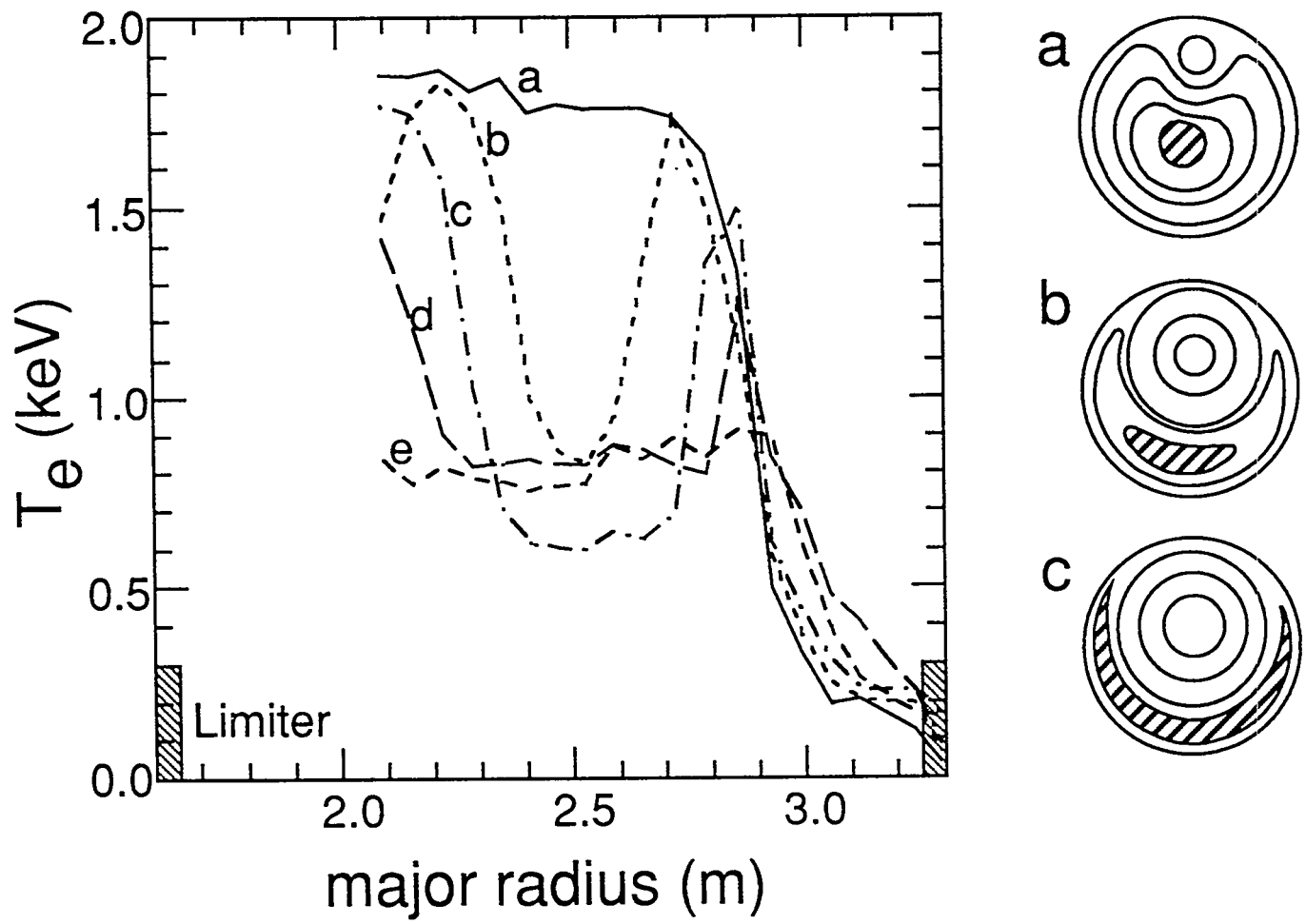


Figure 3a

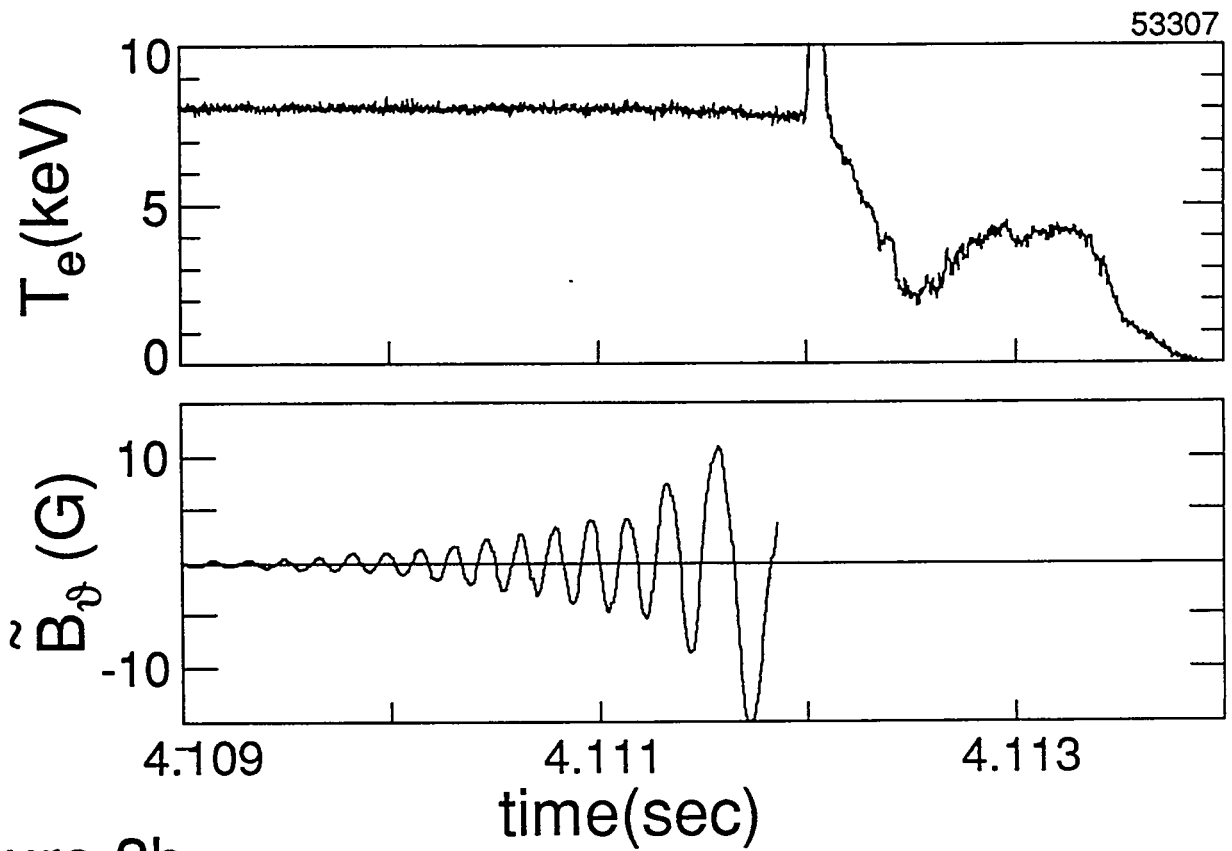


Figure 3b

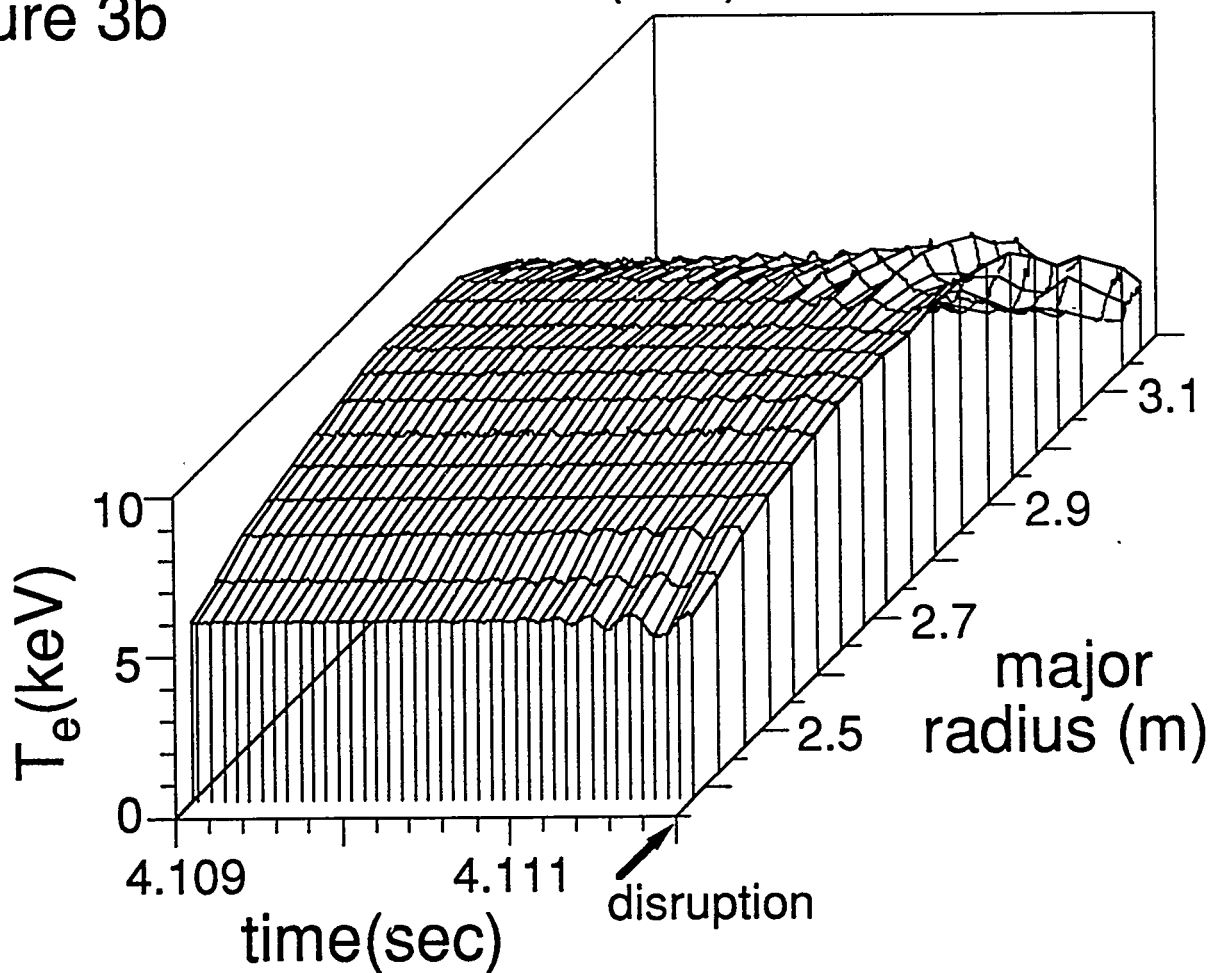


Figure 4a

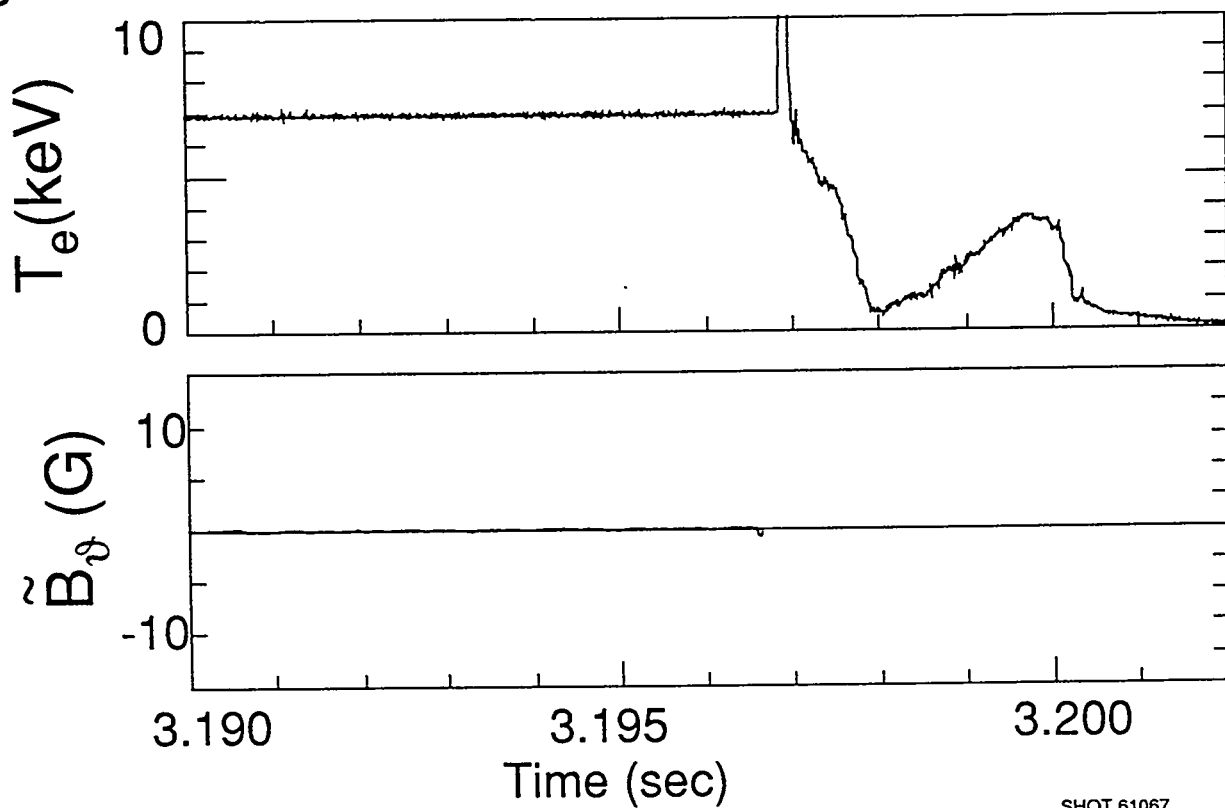


Figure 4b

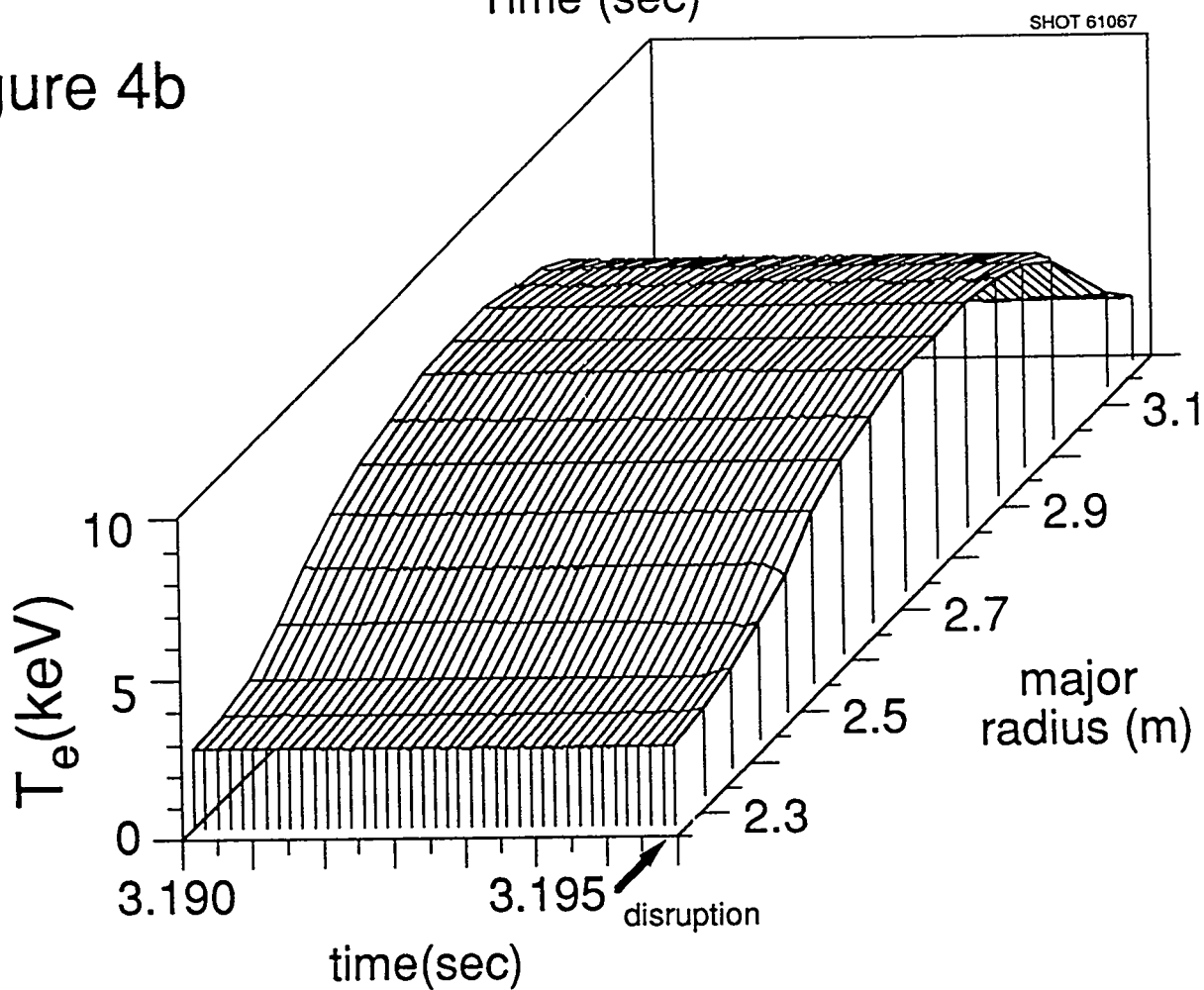


Figure 5

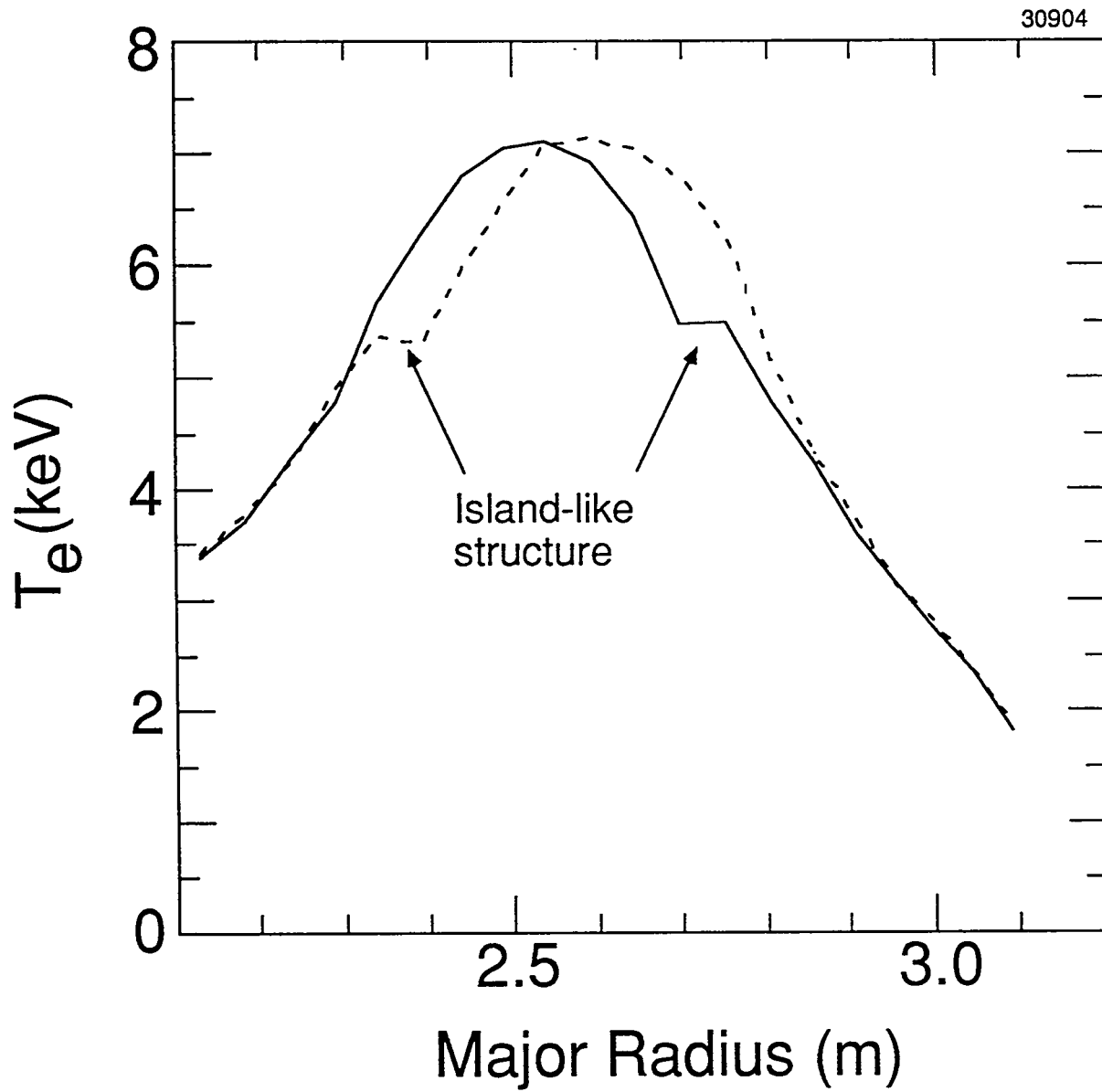
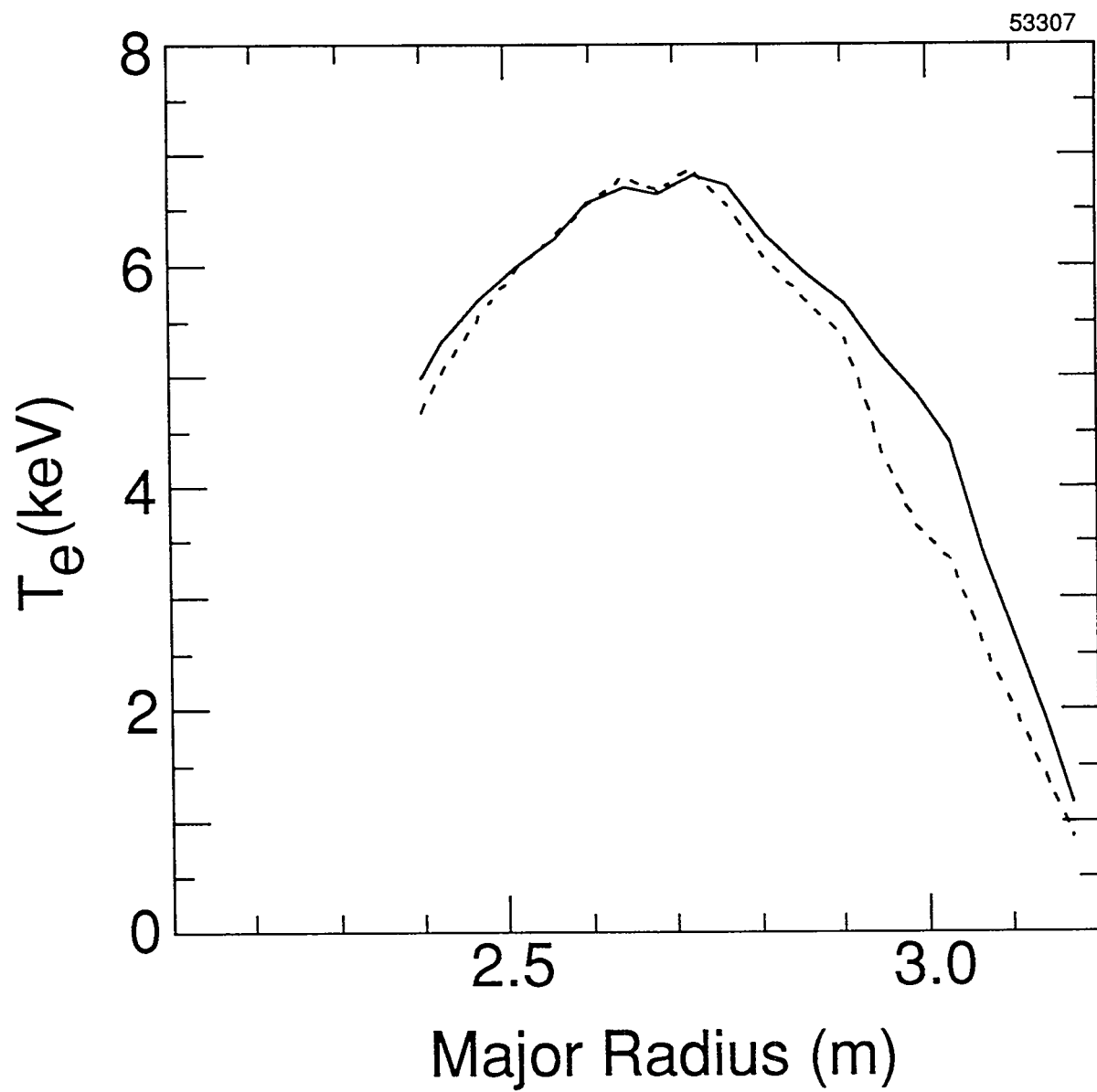


Figure 6



53307

Figure 7

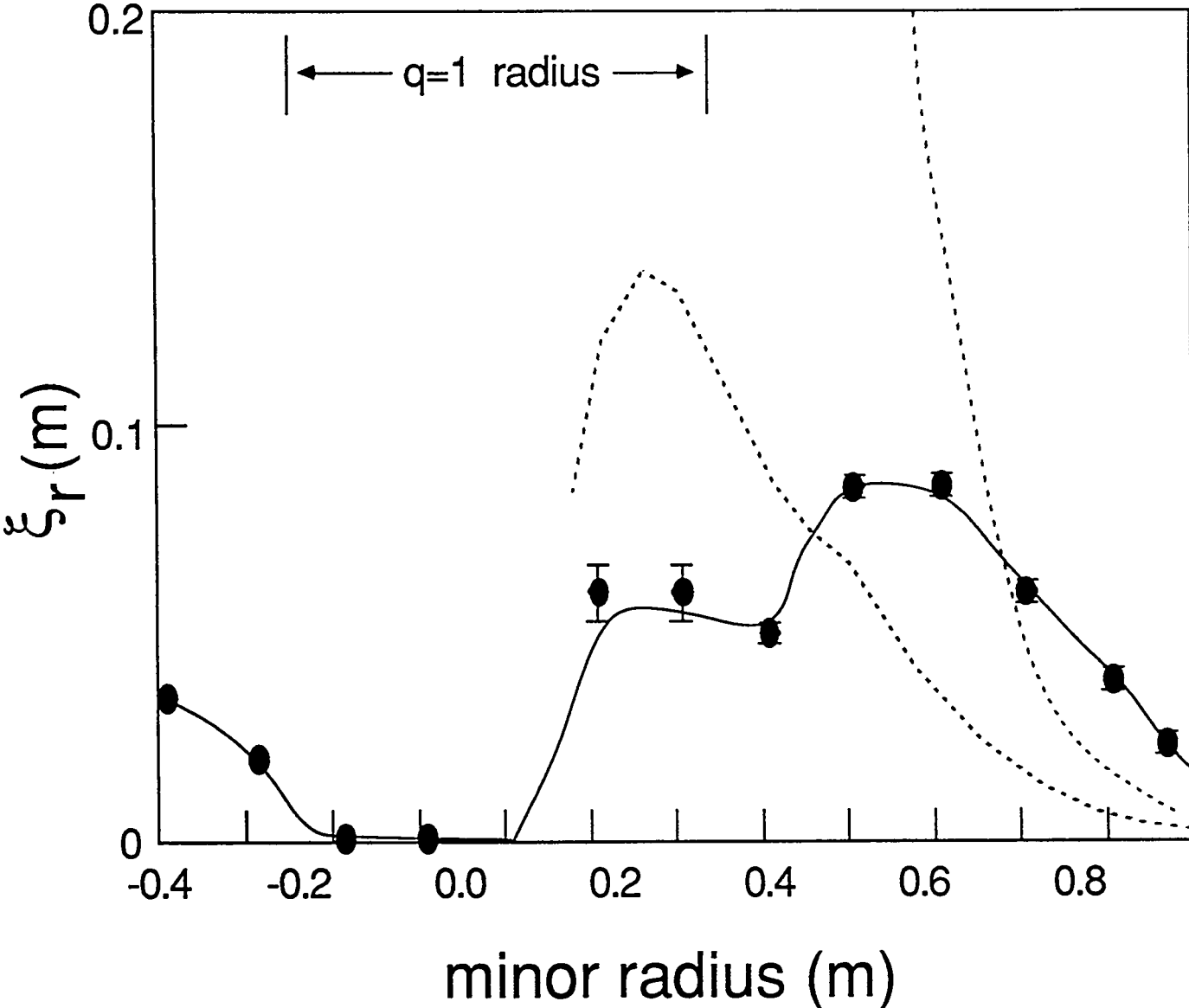


Figure 8

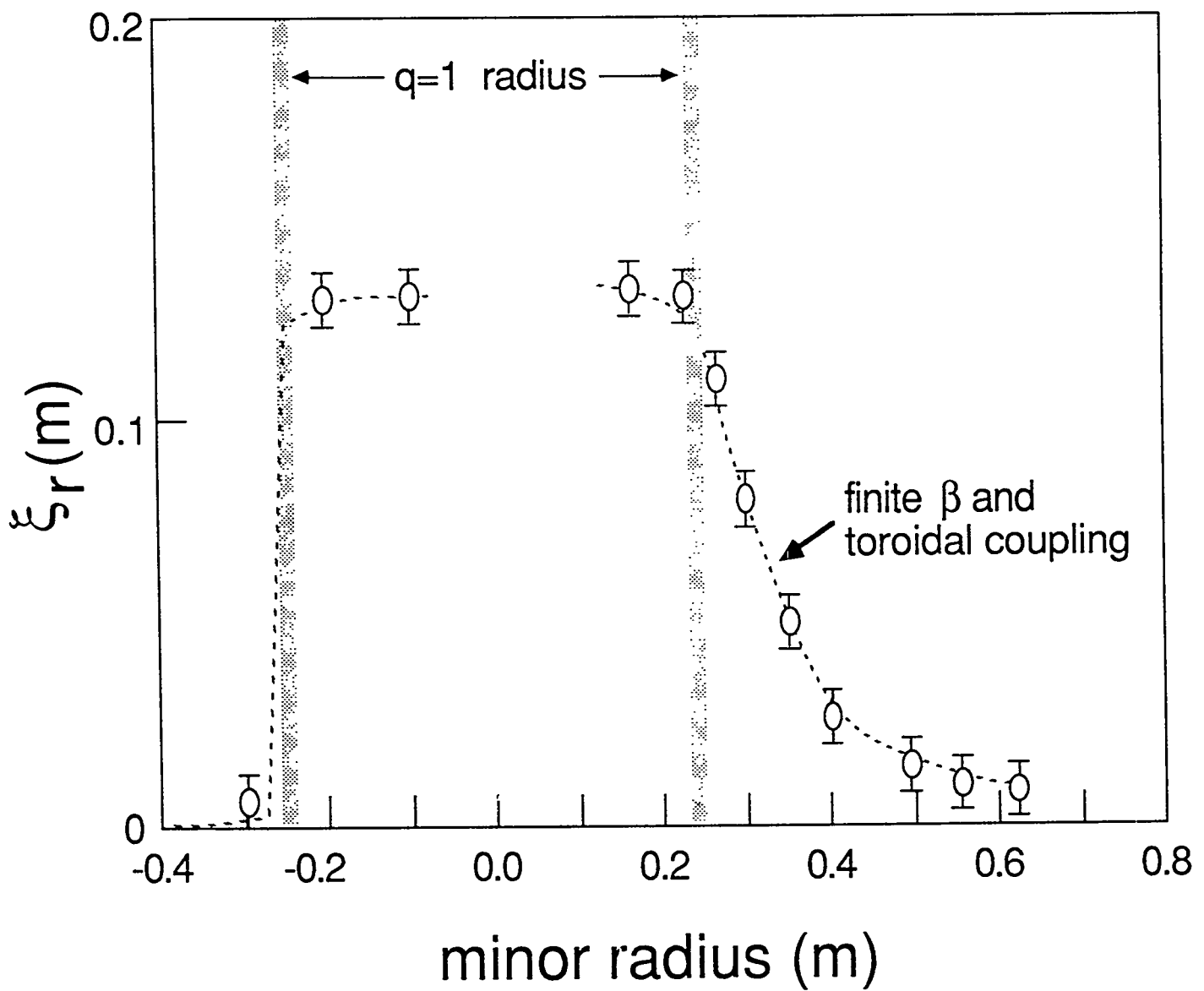


Figure 9

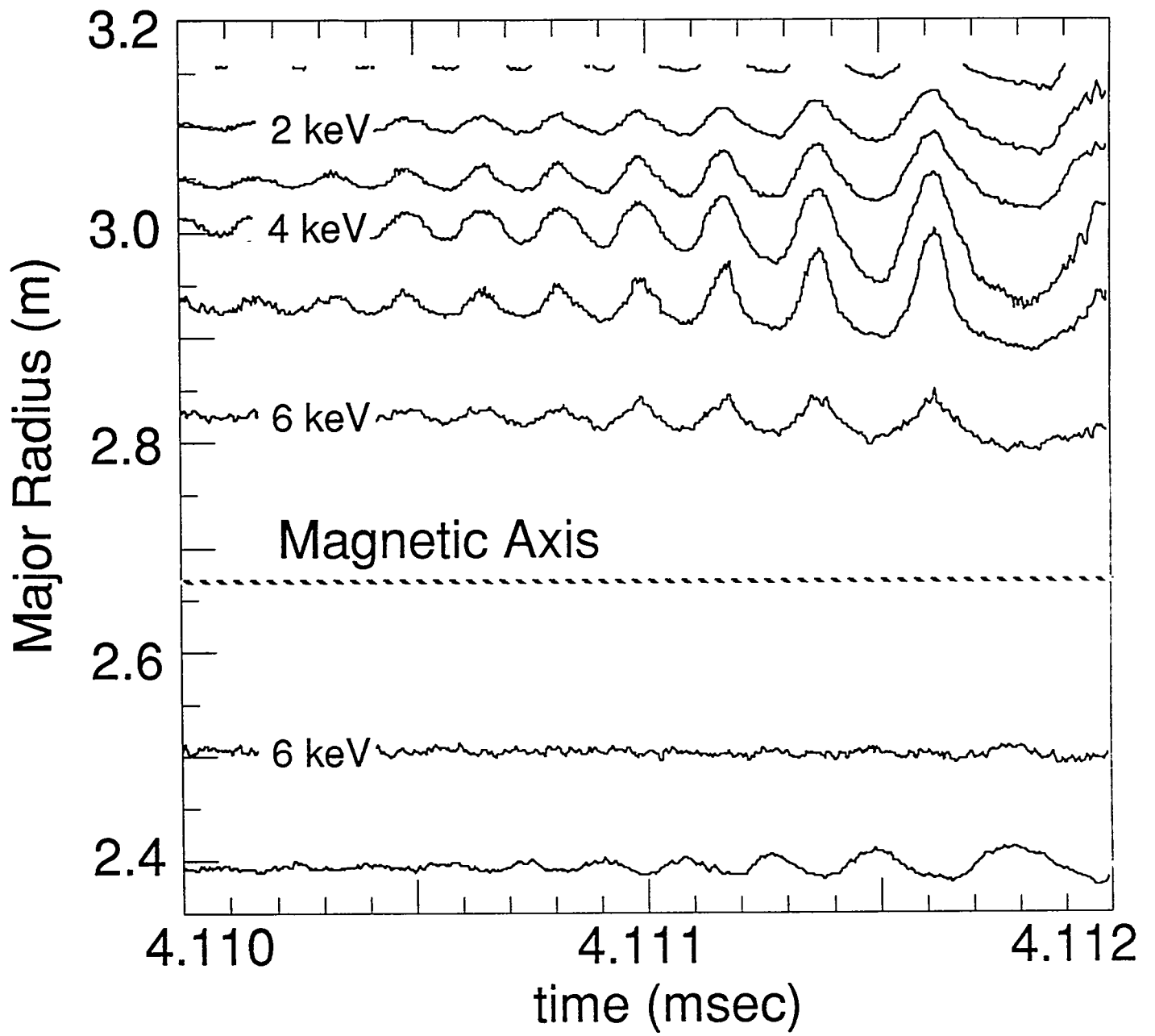


Figure 10a

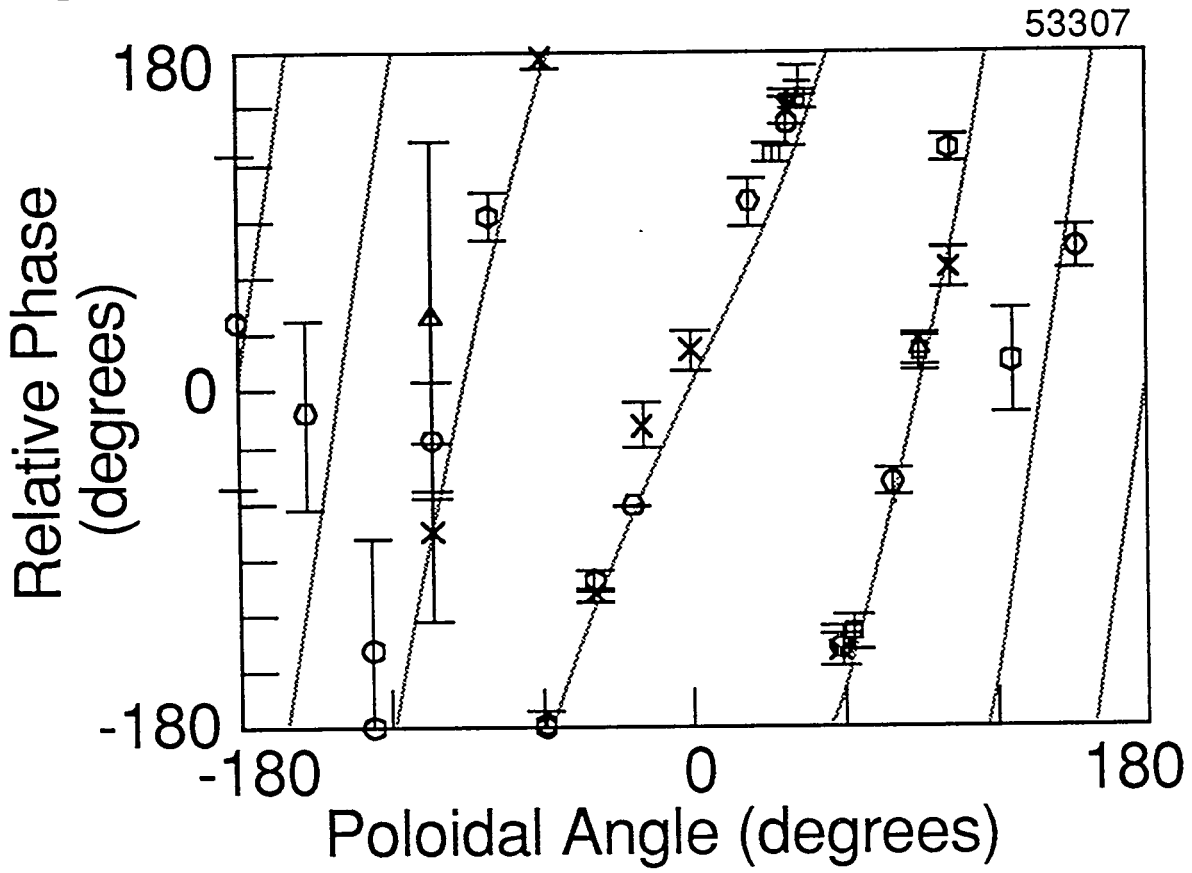
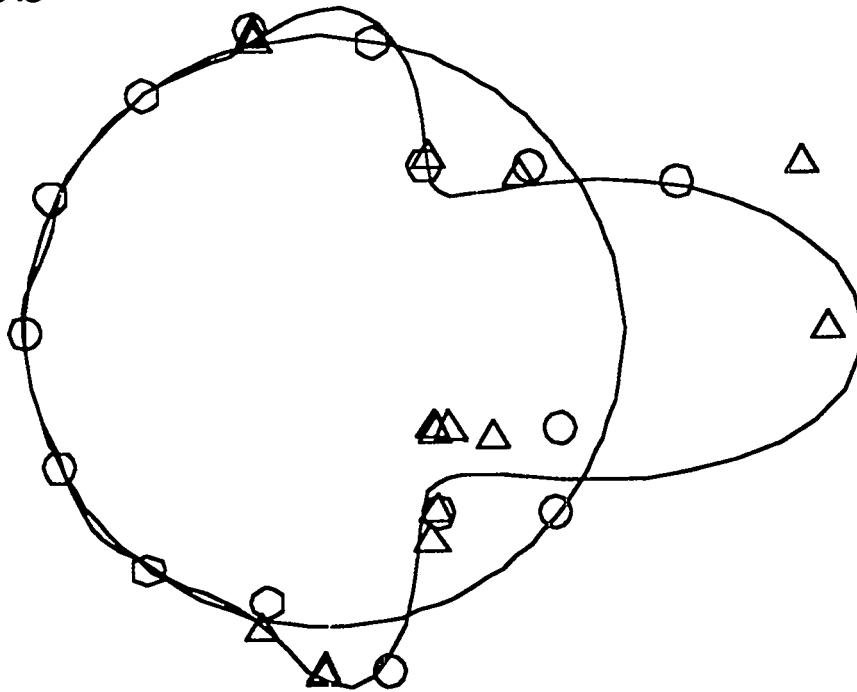
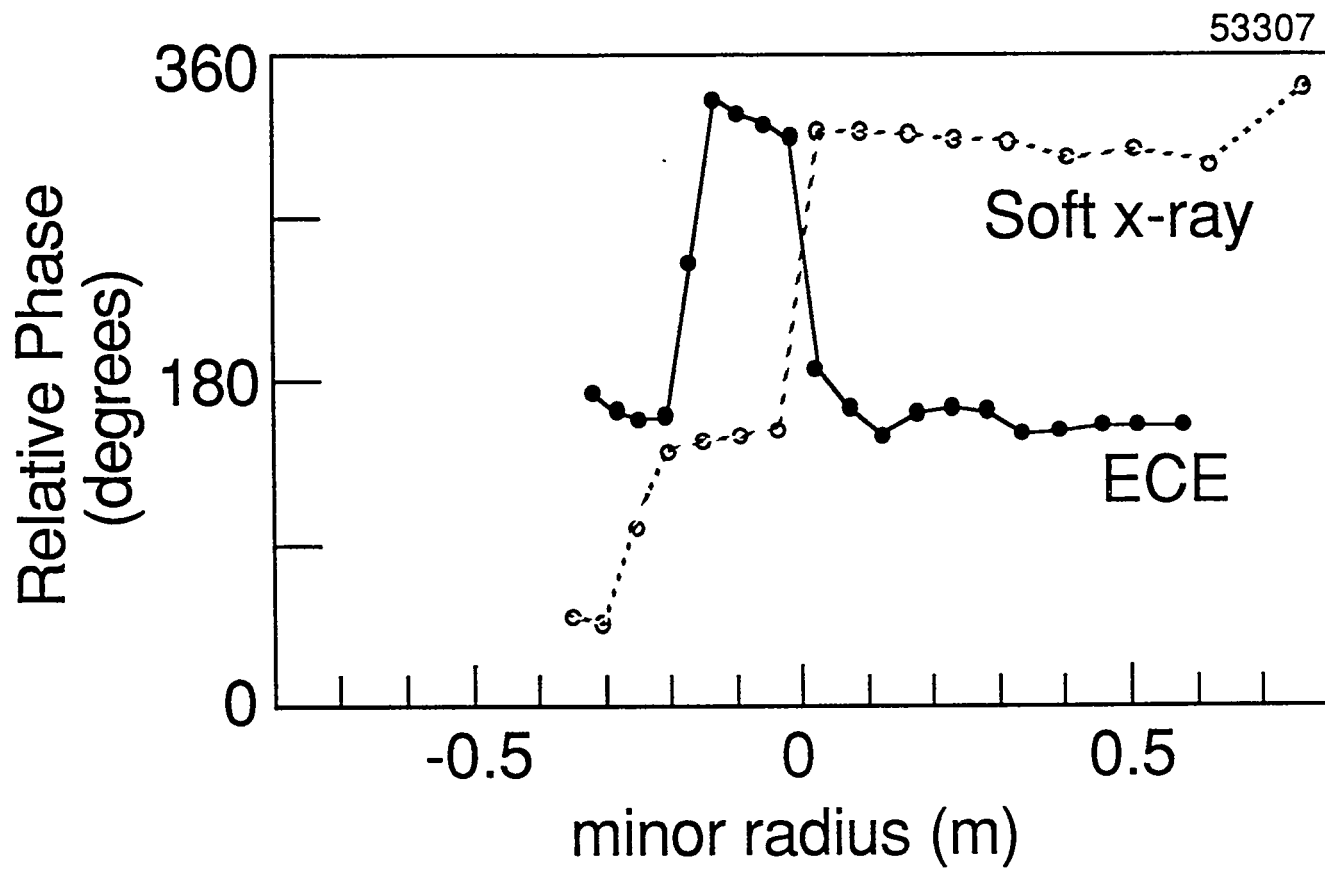


Figure 10b



# Figure 11



# Figure 12

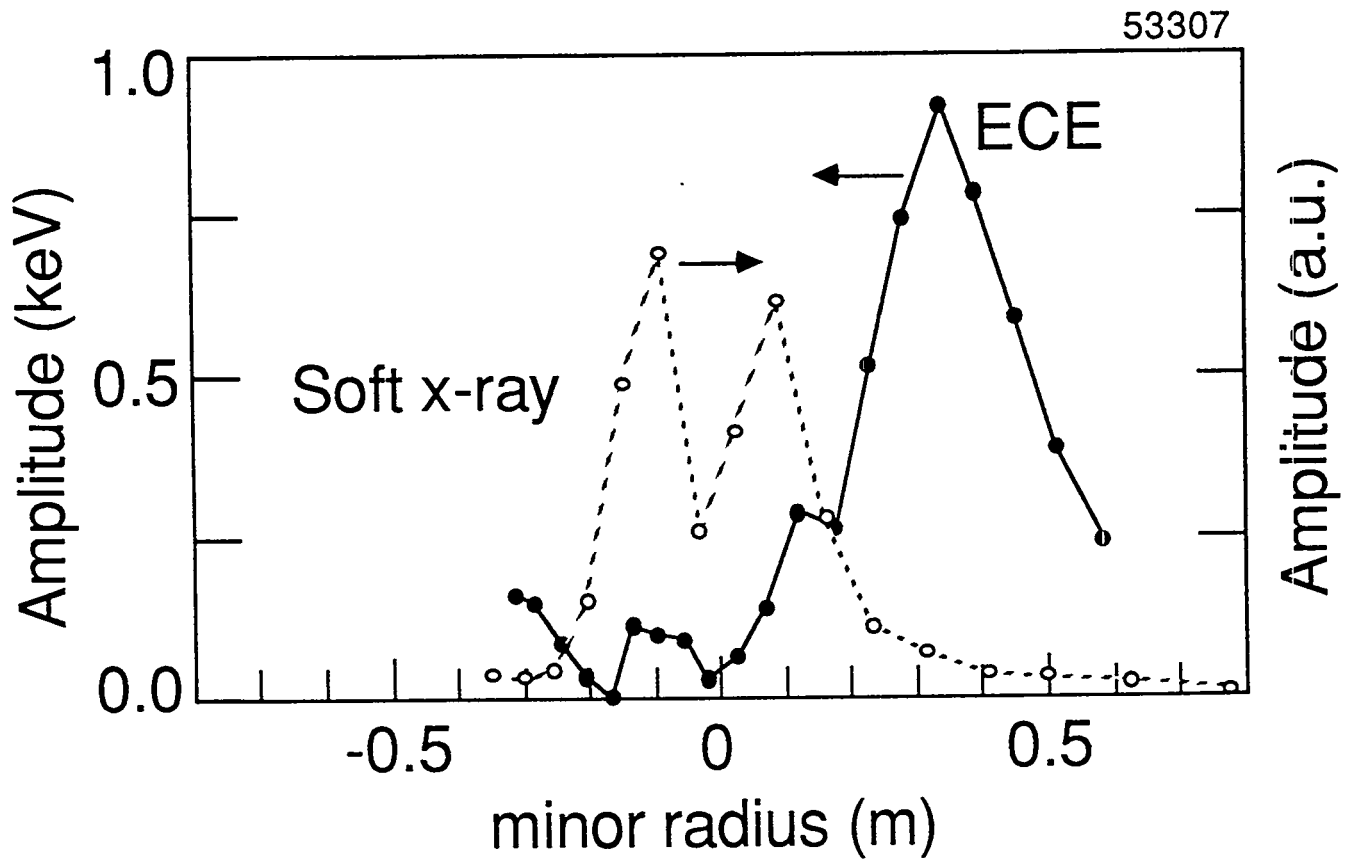


# Figure 13

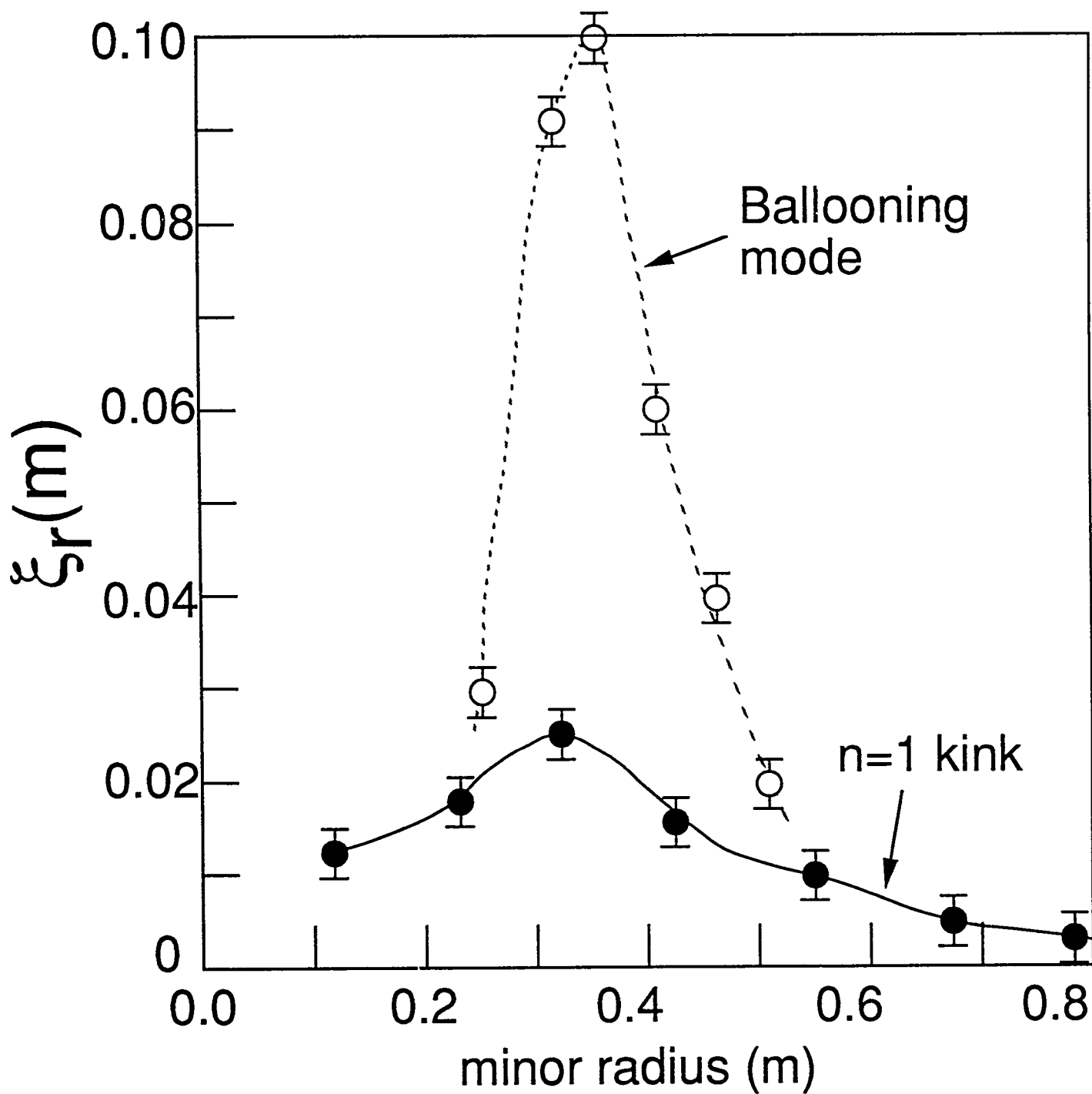


# Figure 14

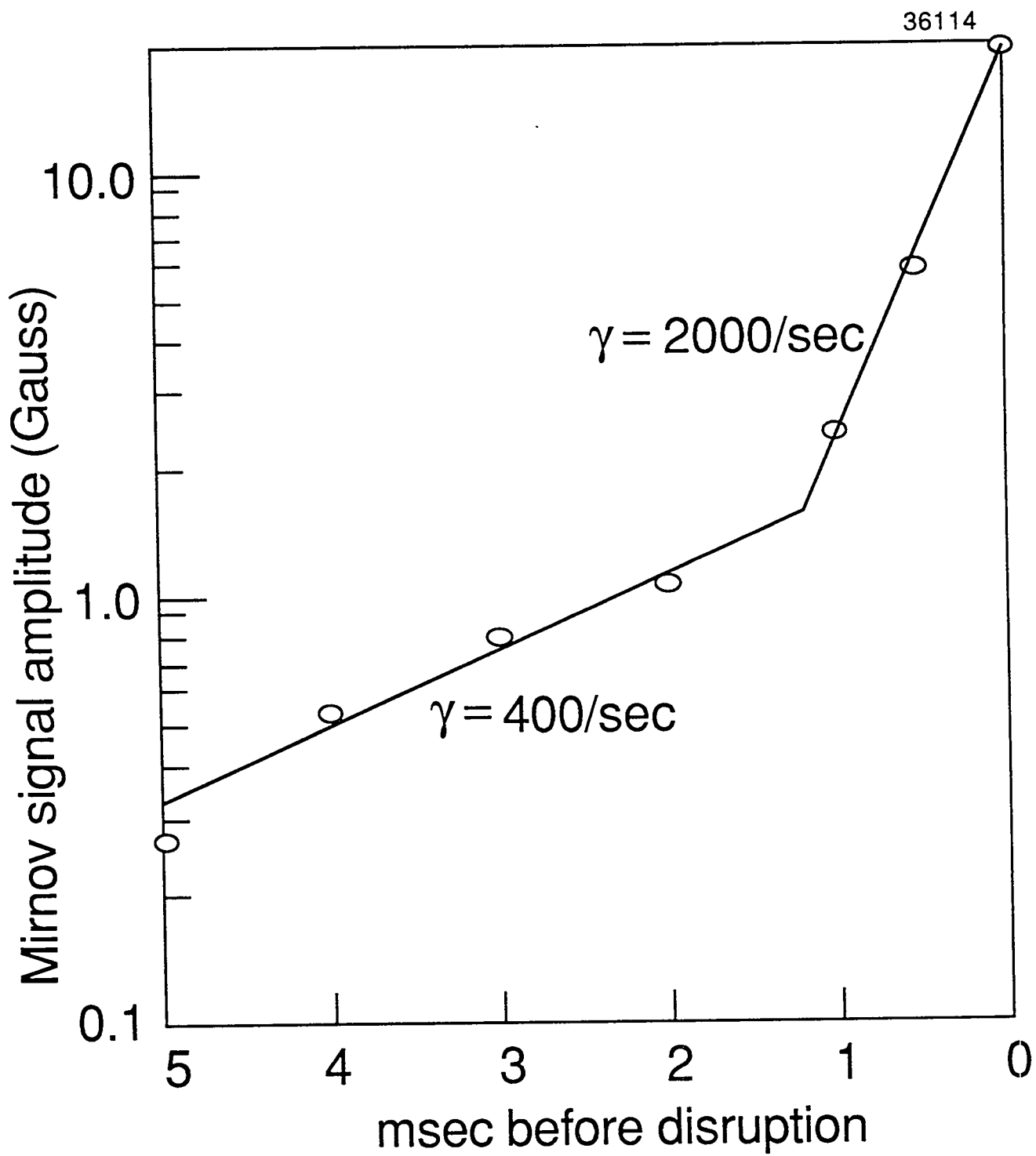


Figure 15a

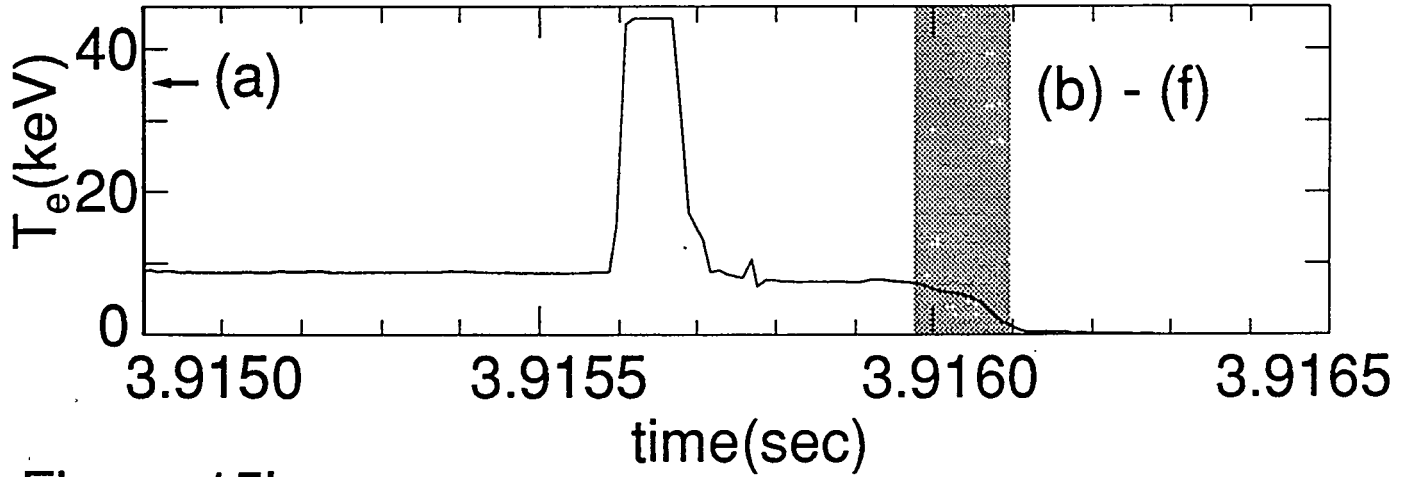


Figure 15b

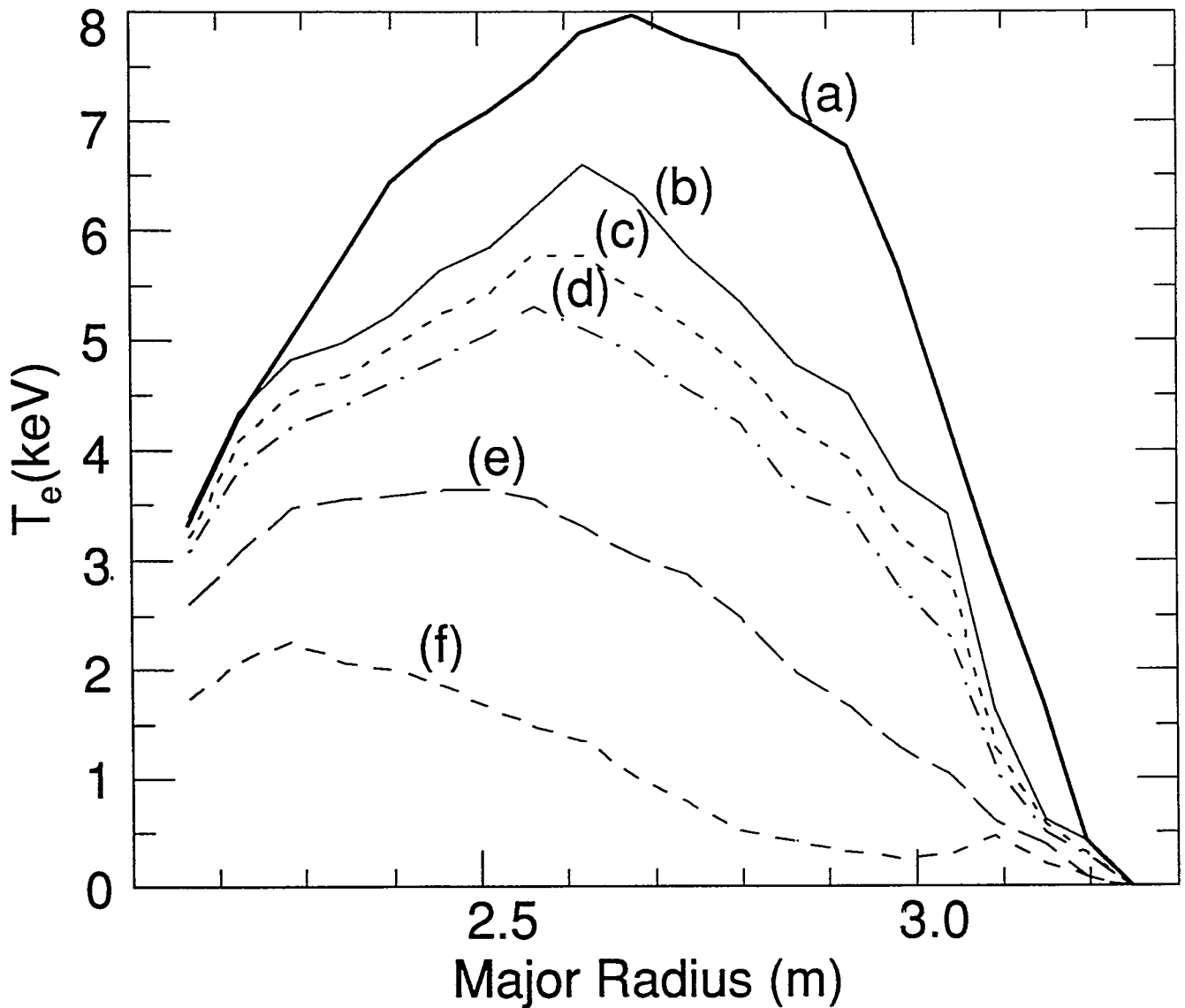


Figure 16

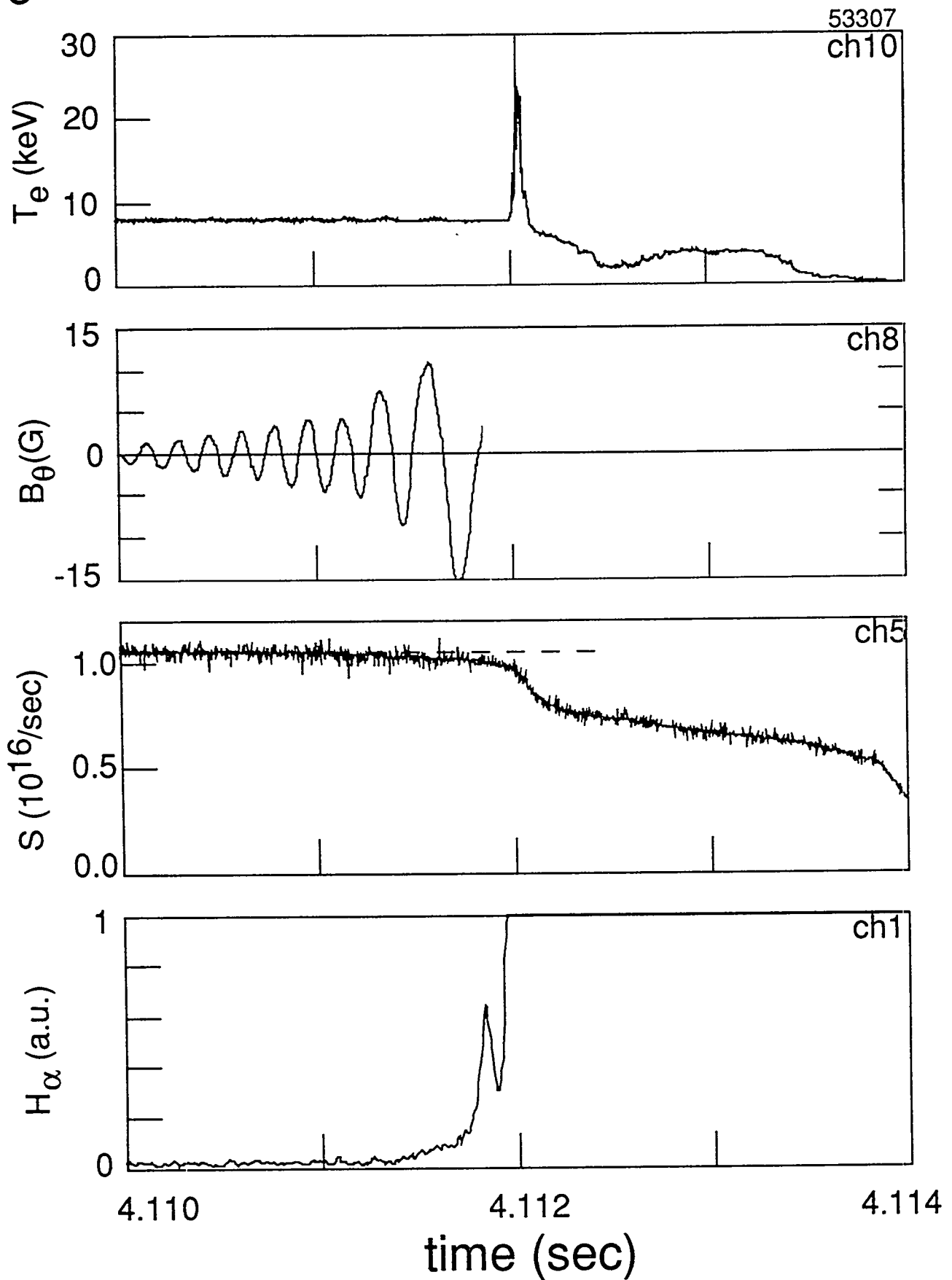


Figure 17

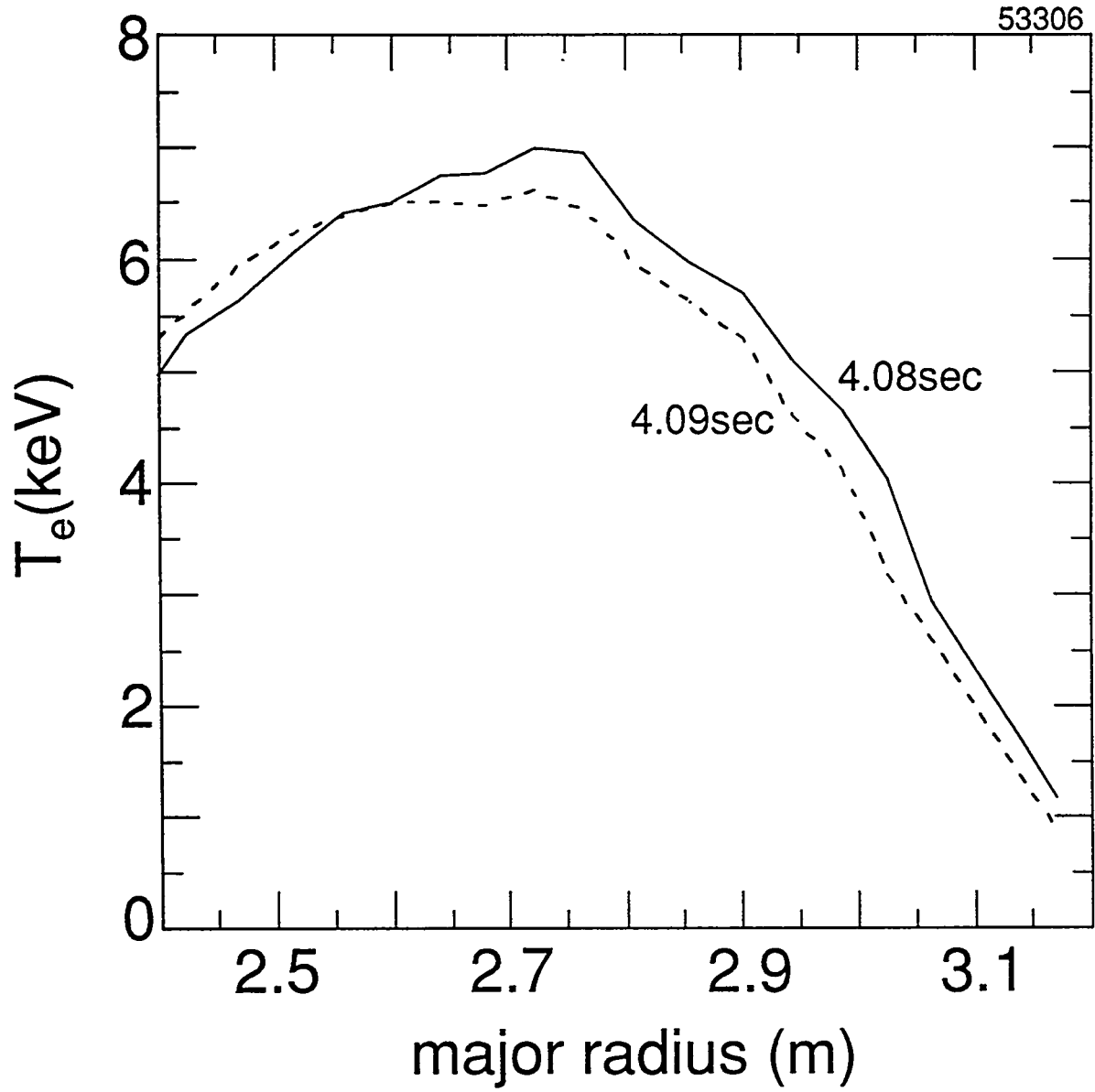


Figure 18

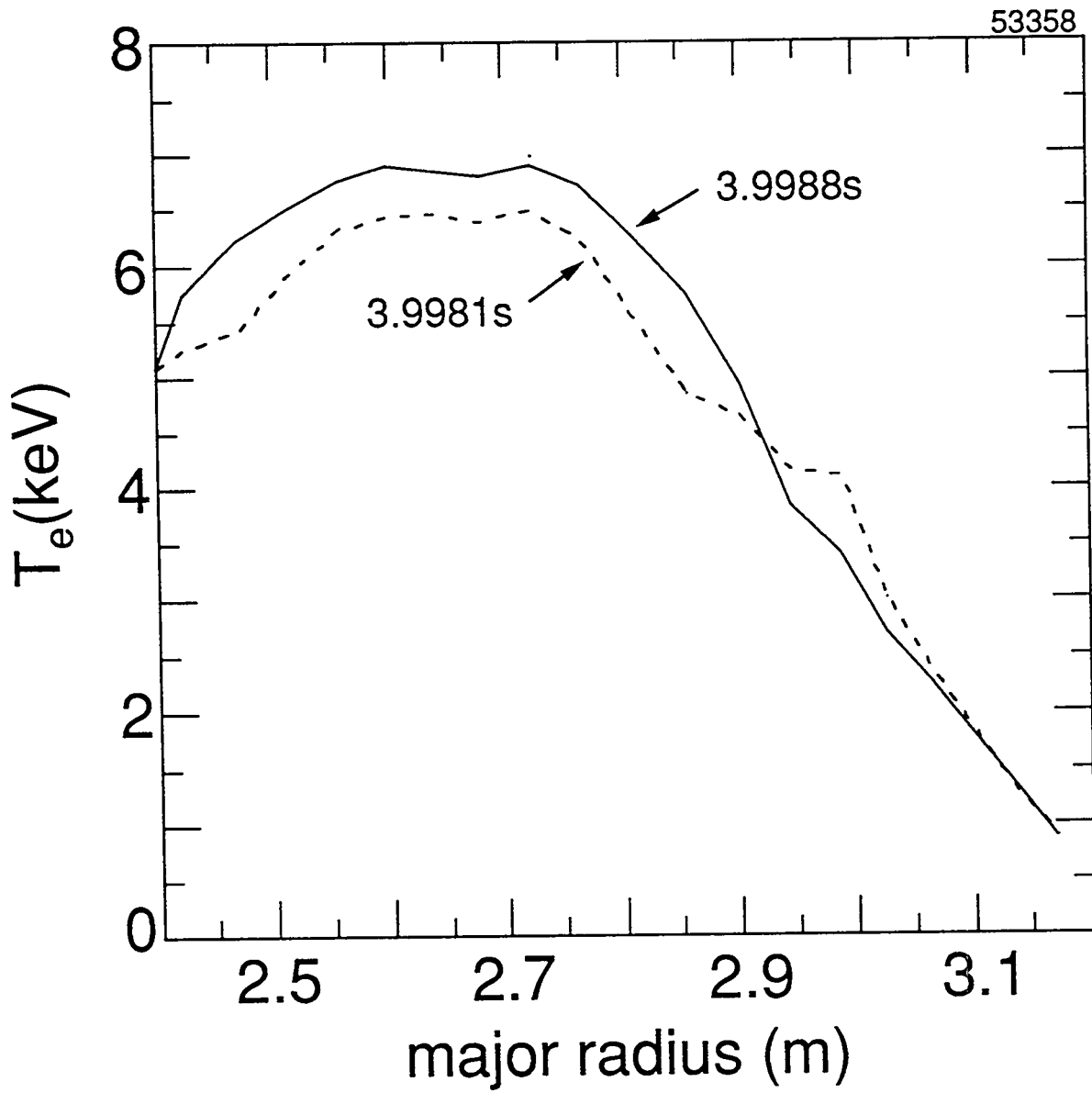


Figure 19

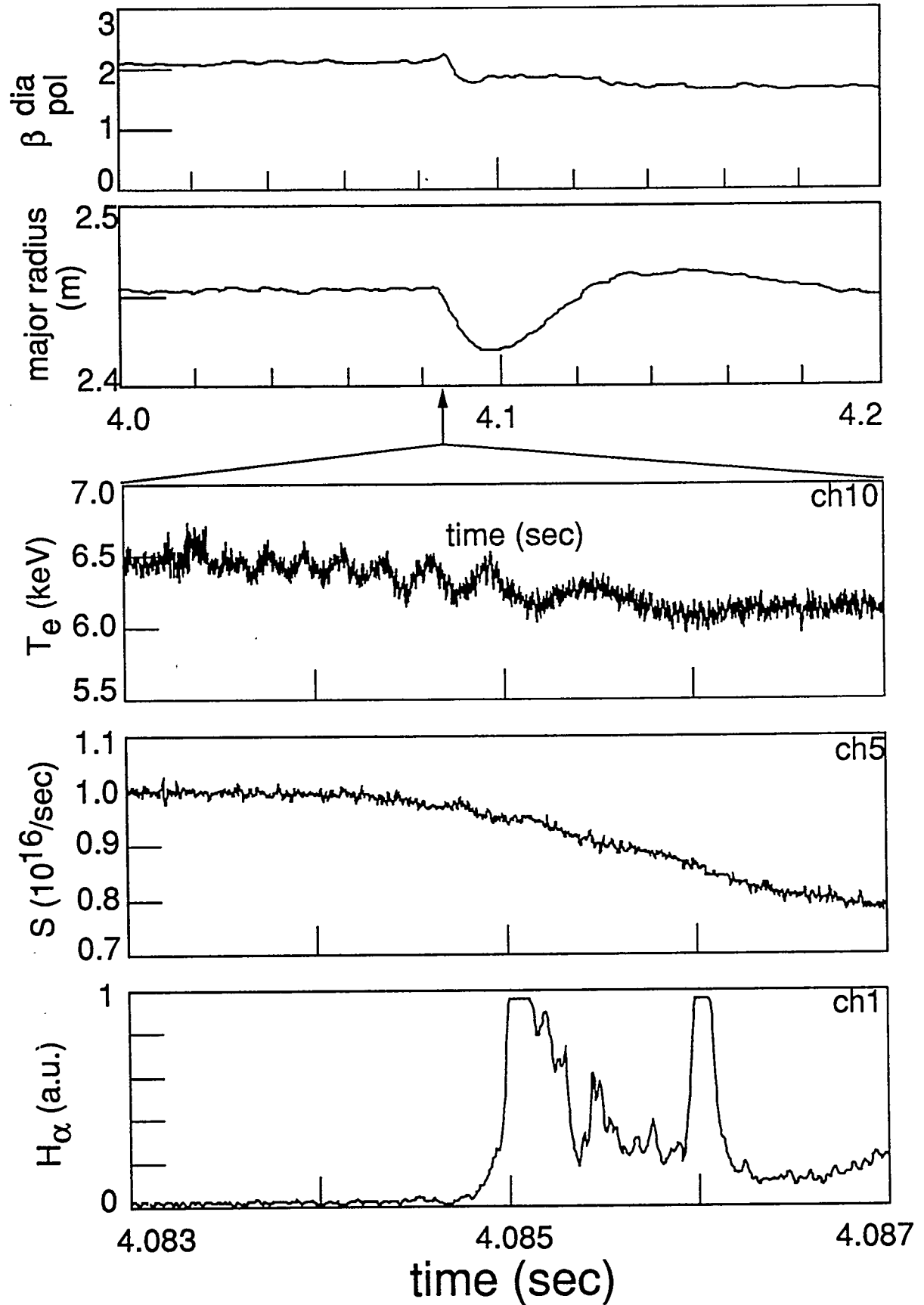


Figure 20

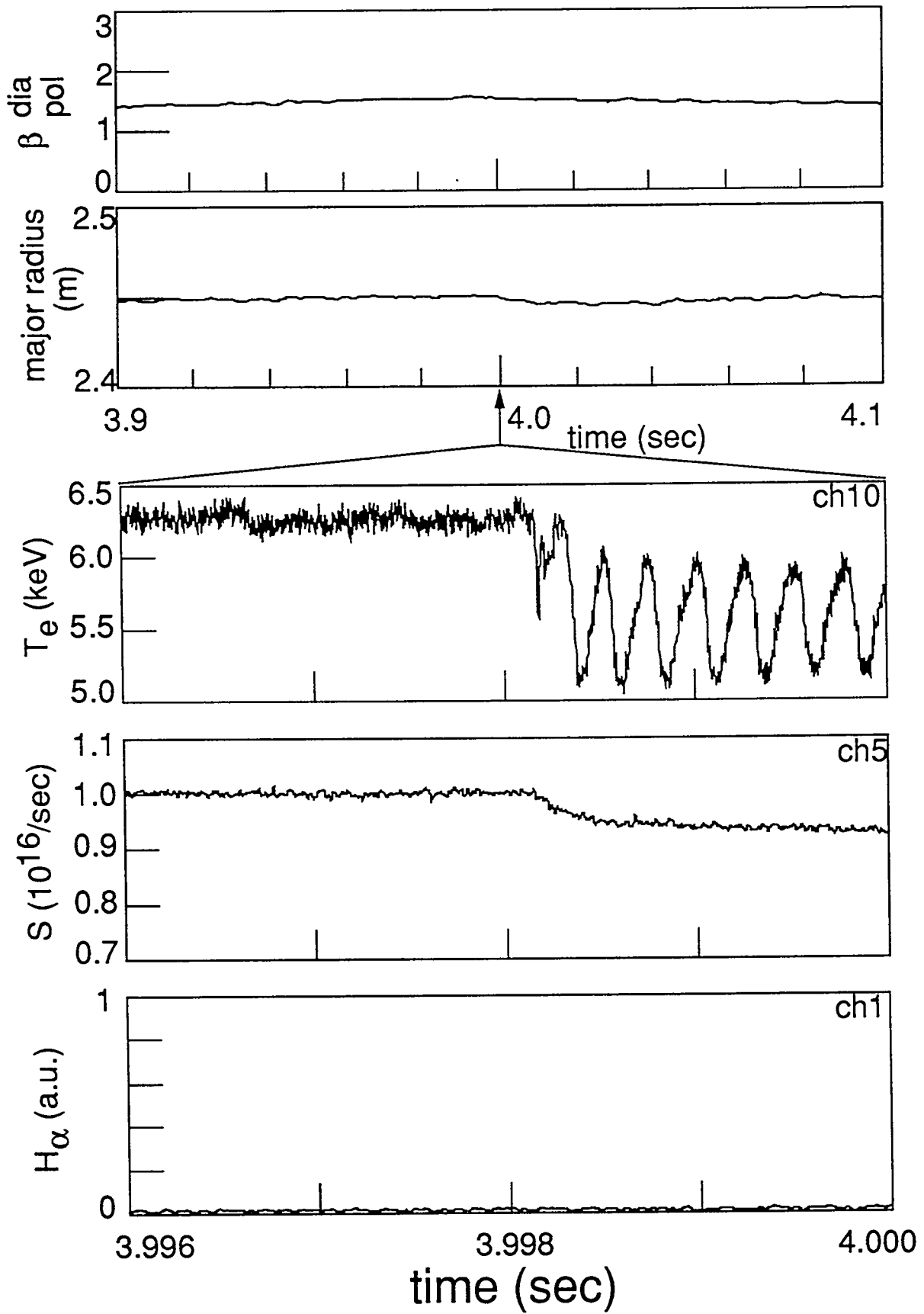


Figure 21

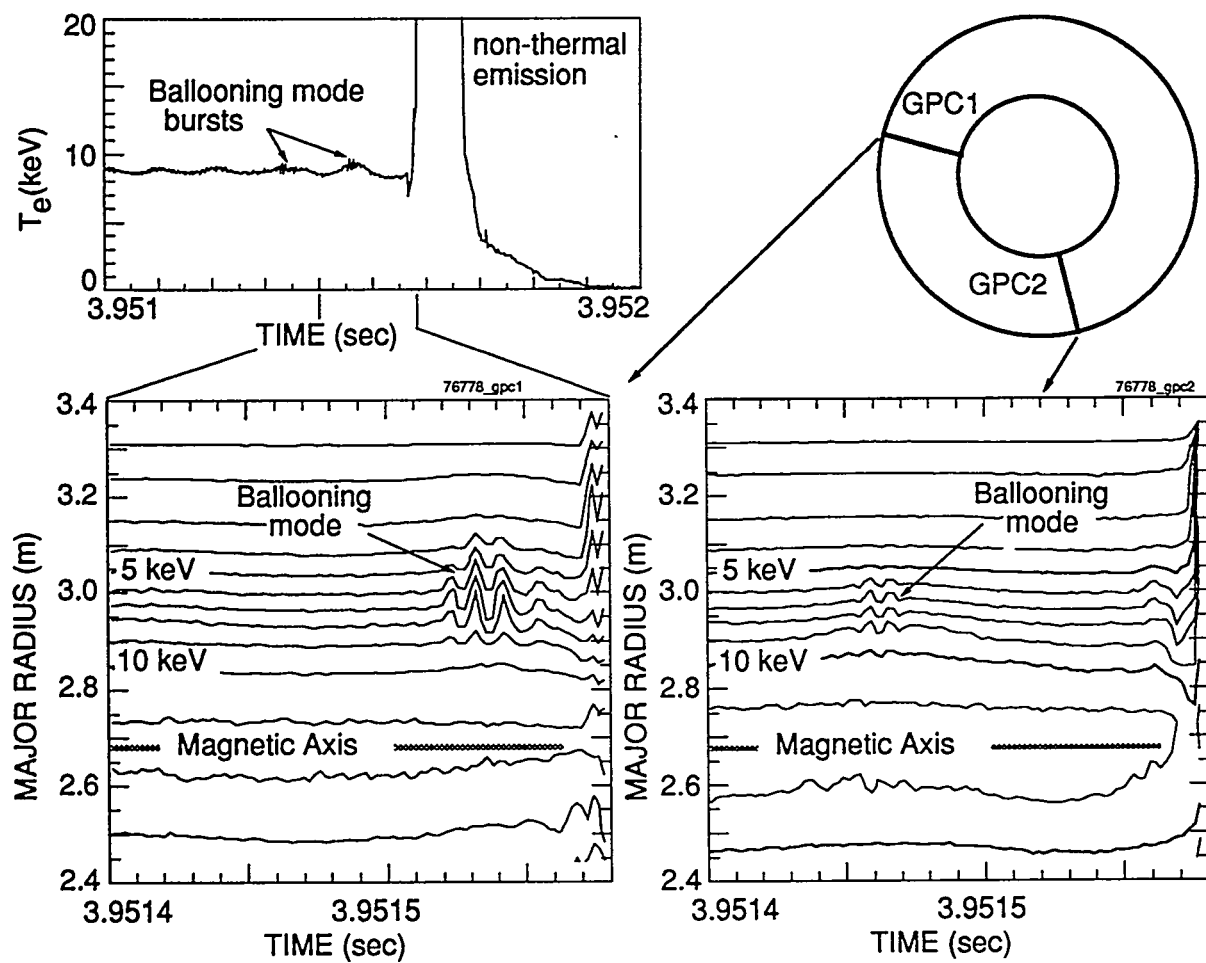
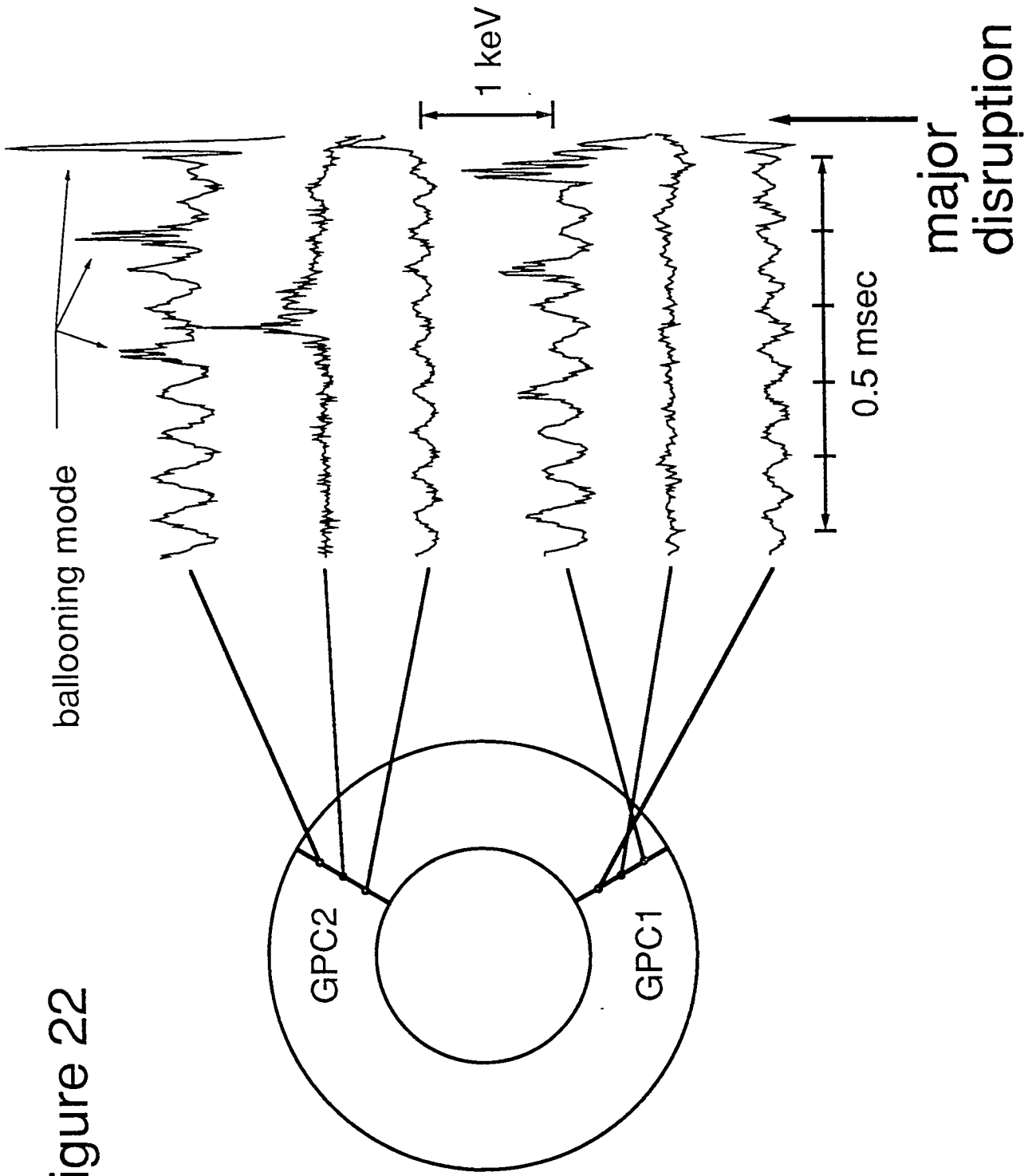


Figure 22



## EXTERNAL DISTRIBUTION IN ADDITION TO UC-420

Dr. F. Paoloni, Univ. of Wollongong, AUSTRALIA  
 Prof. R.C. Cross, Univ. of Sydney, AUSTRALIA  
 Plasma Research Lab., Australian Nat. Univ., AUSTRALIA  
 Prof. I.R. Jones, Flinders Univ, AUSTRALIA  
 Prof. F. Cap, Inst. for Theoretical Physics, AUSTRIA  
 Prof. M. Heindler, Institut für Theoretische Physik, AUSTRIA  
 Prof. M. Goossens, Astronomisch Instituut, BELGIUM  
 Ecole Royale Militaire, Lab. de Phy. Plasmas, BELGIUM  
 Commission-European, DG. XII-Fusion Prog., BELGIUM  
 Prof. R. Bouciqué, Rijksuniversiteit Gent, BELGIUM  
 Dr. P.H. Sakanaka, Instituto Fisica, BRAZIL  
 Prof. Dr. I.C. Nascimento, Instituto Fisica, Sao Paulo, BRAZIL  
 Instituto Nacional De Pesquisas Espaciais-INPE, BRAZIL  
 Documents Office, Atomic Energy of Canada Ltd., CANADA  
 Ms. M. Morin, CCFM/Tokamak de Varennes, CANADA  
 Dr. M.P. Bachynski, MPB Technologies, Inc., CANADA  
 Dr. H.M. Skarsgard, Univ. of Saskatchewan, CANADA  
 Prof. J. Teichmann, Univ. of Montreal, CANADA  
 Prof. S.R. Sreenivasan, Univ. of Calgary, CANADA  
 Prof. R. Marchand, INRS-Energie et Materiaux, CANADA  
 Dr. R. Bolton, Centre canadien de fusion magnétique, CANADA  
 Dr. C.R. James,, Univ. of Alberta, CANADA  
 Dr. P. Lukác, Komenského Univerzita, CZECHO-SLOVAKIA  
 The Librarian, Culham Laboratory, ENGLAND  
 Library, R61, Rutherford Appleton Laboratory, ENGLAND  
 Mrs. S.A. Hutchinson, JET Library, ENGLAND  
 Dr. S.C. Sharma, Univ. of South Pacific, FIJI ISLANDS  
 P. Mähönen, Univ. of Helsinki, FINLAND  
 Prof. M.N. Bussac, Ecole Polytechnique,, FRANCE  
 C. Mouttet, Lab. de Physique des Milieux Ionisés, FRANCE  
 J. Radet, CEN/CADARACHE - Bat 506, FRANCE  
 Prof. E. Economou, Univ. of Crete, GREECE  
 Ms. C. Rinni, Univ. of Ioannina, GREECE  
 Preprint Library, Hungarian Academy of Sci., HUNGARY  
 Dr. B. DasGupta, Saha Inst. of Nuclear Physics, INDIA  
 Dr. P. Kaw, Inst. for Plasma Research, INDIA  
 Dr. P. Rosenau, Israel Inst. of Technology, ISRAEL  
 Librarian, International Center for Theo Physics, ITALY  
 Miss C. De Palo, Associazione EURATOM-ENEA , ITALY  
 Dr. G. Grosso, Istituto di Fisica del Plasma, ITALY  
 Prof. G. Rostangni, Istituto Gas Ionizzati Del Cnr, ITALY  
 Dr. H. Yamato, Toshiba Res & Devel Center, JAPAN  
 Prof. I. Kawakami, Hiroshima Univ., JAPAN  
 Prof. K. Nishikawa, Hiroshima Univ., JAPAN  
 Librarian, Naka Fusion Research Establishment, JAERI, JAPAN  
 Director, Japan Atomic Energy Research Inst., JAPAN  
 Prof. S. Itoh, Kyushu Univ., JAPAN  
 Research Info. Ctr., National Instit. for Fusion Science, JAPAN  
 Prof. S. Tanaka, Kyoto Univ., JAPAN  
 Library, Kyoto Univ., JAPAN  
 Prof. N. Inoue, Univ. of Tokyo, JAPAN  
 Secretary, Plasma Section, Electrotechnical Lab., JAPAN  
 Dr. O. Mitarai, Kumamoto Inst. of Technology, JAPAN  
 Dr. G.S. Lee, Korea Basic Sci. Ctr., KOREA  
 J. Hyeon-Sook, Korea Atomic Energy Research Inst., KOREA  
 D.I. Choi, The Korea Adv. Inst. of Sci. & Tech., KOREA  
 Prof. B.S. Liley, Univ. of Waikato, NEW ZEALAND  
 Inst of Physics, Chinese Acad Sci PEOPLE'S REP. OF CHINA  
 Library, Inst. of Plasma Physics, PEOPLE'S REP. OF CHINA  
 Tsinghua Univ. Library, PEOPLE'S REPUBLIC OF CHINA  
 Z. Li, S.W. Inst Physics, PEOPLE'S REPUBLIC OF CHINA  
 Prof. J.A.C. Cabral, Instituto Superior Tecnico, PORTUGAL  
 Prof. M.A. Hellberg, Univ. of Natal, S. AFRICA  
 Prof. D.E. Kim, Pohang Inst. of Sci. & Tech., SO. KOREA  
 Prof. C.I.E.M.A.T, Fusion Division Library, SPAIN  
 Dr. L. Stenflo, Univ. of UMEA, SWEDEN  
 Library, Royal Inst. of Technology, SWEDEN  
 Prof. H. Wilhelmson, Chalmers Univ. of Tech., SWEDEN  
 Centre Phys. Des Plasmas, Ecole Polytech, SWITZERLAND  
 Bibliotheek, Inst. Voor Plasma-Fysica, THE NETHERLANDS  
 Asst. Prof. Dr. S. Cakir, Middle East Tech. Univ., TURKEY  
 Dr. V.A. Glukhikh, Sci. Res. Inst. Electrophys.I Apparatus, USSR  
 Dr. D.D. Ryutov, Siberian Branch of Academy of Sci., USSR  
 Dr. G.A. Eliseev, I.V. Kurchatov Inst., USSR  
 Librarian, The Ukr.SSR Academy of Sciences, USSR  
 Dr. L.M. Kovrizhnykh, Inst. of General Physics, USSR  
 Kernforschungsanlage GmbH, Zentralbibliothek, W. GERMANY  
 Bibliothek, Inst. Für Plasmaforschung, W. GERMANY  
 Prof. K. Schindler, Ruhr-Universität Bochum, W. GERMANY  
 Dr. F. Wagner, (ASDEX), Max-Planck-Institut, W. GERMANY  
 Librarian, Max-Planck-Institut, W. GERMANY